nature medicine

MitoNEET-driven alterations in adipocyte mitochondrial activity reveal a crucial adaptive process that preserves insulin sensitivity in obesity

Christine M Kusminski[1], William L Holland[1], Kai Sun[1], Jiyoung Park[1], Stephen B Spurgin[1], Ying Lin[2], G Roger Askew[3], Judith A Simcox[4], Don A McClain[4,5], Cai Li[3] & Philipp E Scherer[1,6]

We examined mouse models with altered adipocyte expression of mitoNEET, a protein residing in the mitochondrial outer membrane, to probe its impact on mitochondrial function and subsequent cellular responses. We found that overexpression of mitoNEET enhances lipid uptake and storage, leading to an expansion of the mass of adipose tissue. Despite the resulting massive obesity, benign aspects of adipose tissue expansion prevail, and insulin sensitivity is preserved. Mechanistically, we also found that mitoNEET inhibits mitochondrial iron transport into the matrix and, because iron is a rate-limiting component for electron transport, lowers the rate of β-oxidation. This effect is associated with a lower mitochondrial membrane potential and lower levels of reactive oxygen species–induced damage, along with increased production of adiponectin. Conversely, a reduction in mitoNEET expression enhances mitochondrial respiratory capacity through enhanced iron content in the matrix, ultimately corresponding to less weight gain on a high-fat diet. However, this reduction in mitoNEET expression also causes heightened oxidative stress and glucose intolerance. Thus, manipulation of mitochondrial function by varying mitoNEET expression markedly affects the dynamics of cellular and whole-body lipid homeostasis.

Over the past decade, efforts have focused on the connection between mitochondrial activity and the etiology of obesity, insulin resistance and the progression of type 2 diabetes mellitus (T2DM)[1,2]. Numerous studies have shown that metabolic disorders are accompanied by reduced mitochondrial content, compromised mitochondrial respiratory capacity, heightened oxidative stress and, consequently, altered whole-body lipid and glucose metabolism[3,4]. The mechanisms that prompt the compromised mitochondrial activity in obesity-driven T2DM and how targeting these processes can improve metabolic profiles remain largely unknown. New preclinical models that elucidate a role for mitochondria in cellular homeostasis have the potential to shed new light on these issues and will allow the discovery of improved therapeutic avenues.

The expansion of healthy adipose tissue has potent antidiabetic effects because it provides a 'safe haven' to neutralize and store excess free fatty acids (FFAs) that would otherwise cause toxicity to other, more sensitive organs that regulate whole-body metabolism. Thus, the inability to appropriately expand subcutaneous white adipose tissue (sWAT) may underlie the development of insulin resistance, β cell failure and T2DM[5]. In addition to storing excess lipids, however, adipocytes can also secrete adipokines that help buffer the lipotoxic side effects of excess caloric intake. A crucial player in this regard is adiponectin. Secreted exclusively from adipocytes, adiponectin promotes the preferential storage of triglycerides in adipose tissue[5,6] to improve metabolic flexibility. Adiponectin further reduces the accumulation of ceramide species to improve cellular survival and insulin sensitivity. Mice overexpressing adiponectin in an *ob*/*ob* background have improved insulin sensitivity and lipid profiles compared to *ob*/*ob* mice that have normal obesity-associated downregulation of adiponectin[5]. Such characteristics are attributed to augmented ceramidase activity[7], a redistribution of lipids and higher adipogenesis concomitant with gross sWAT expansion[5,6]. However, the underlying mechanisms that initiate this paradoxical phenomenon of lipid redistribution and chronic adipose tissue expansion to improve metabolic health are not fully defined.

Mitochondria have a central role in energy homeostasis by partitioning fuels toward β-oxidation or storage as fat. During adipose tissue expansion, the oxidation of lipid and carbohydrate fuels requires the coordinated regulation of downstream metabolic pathways such as the tricarboxylic acid cycle and the electron transport chain (ETC). Compromised mitochondrial energy production is a major anomaly in obesity. In particular, obese individuals and those with type 2 diabetes are known to have lower β-oxidation rates, lower oxidative enzymatic activities and lower ETC activity[8,9] together with greater glycolytic capacities and higher uptake of cellular fatty acids compared to nonobese and nondiabetic individuals[10]. Although these

[1]Touchstone Diabetes Center, Department of Internal Medicine, University of Texas Southwestern Medical Center, Dallas, Texas, USA. [2]Department of Cell Biology, Albert Einstein College of Medicine, Bronx, New York, USA. [3]Department of Metabolic Disorders, Merck Research Laboratories, Rahway, New Jersey, USA. [4]Department of Medicine and Biochemistry, University of Utah School of Medicine, Salt Lake City, Utah, USA. [5]Research Service, Virginia Medical Center, Salt Lake City, Utah, USA. [6]Department of Cell Biology, University of Texas Southwestern Medical Center, Dallas, Texas, USA. Correspondence should be addressed to P.E.S. (philipp.scherer@utsouthwestern.edu).

Received 19 March; accepted 10 July; published online 9 September 2012; doi:10.1038/nm.2899

observations highlight oxidative failure during lipid accumulation, the mechanisms by which diminished β-oxidation and suboptimal mitochondrial function stimulate lipid uptake and accumulation in obesity have not been fully established.

Here we take advantage of the unique properties of the mitochondrial membrane protein mitoNEET. Using gain-of-function and loss-of-function models for mitoNEET, we induced chronic and massive adipose tissue expansion, at least partially through an upregulation of adiponectin production and release from adipocytes. MitoNEET achieves these effects through selective modulation of mitochondrial electron transport activity. This establishes a tight functional connection between mitoNEET, mitochondrial activity and adiponectin release.

Originally, mitoNEET was identified as a unique dimeric mitochondrial membrane target crosslinked to the thiazolidinedione (TZD) pioglitazone[11,12]. Located in the outer mitochondrial membrane, mitoNEET was named according to its C-terminal amino acid sequence, AsnGluGluThr (NEET)[11]. Furthermore, oriented toward the cytoplasm, the CDGSH domain of mitoNEET can bind redox-active, pH-labile clusters made up of two iron ions and two sulfur ions (2Fe-2S clusters)[13–15], with pioglitazone having been reported to stabilize the protein against 2Fe-2S cluster release[12]. MitoNEET achieves its effects on cellular and systemic metabolic homeostasis by acting as a powerful regulator of mitochondrial iron content. We used these properties to influence mitochondrial bioenergetics and metabolism in a tissue-type– and cell-type–specific manner, resulting in alterations in whole-body energy homeostasis and, further, opening up new avenues for cell-specific manipulation of mitochondrial activity in any cell type.

RESULTS

MitoNEET promotes gross adipose tissue expansion

Mice can be metabolically challenged by either introducing specific genetic mutations or providing them with a high-fat diet (HFD). An examination of tissues from mice exposed to HFD revealed that their expression of the mitochondrial protein mitoNEET is markedly lower in adipose tissue and the liver compared to its expression in these tissues in mice fed a standard chow diet (**Fig. 1a**), indicating that altered mitoNEET expression may be a hallmark of metabolically challenged tissues.

To address more directly whether mitoNEET activity has a pertinent role in adipose tissue function, we used the 5.4-kb aP2 promoter[16] to

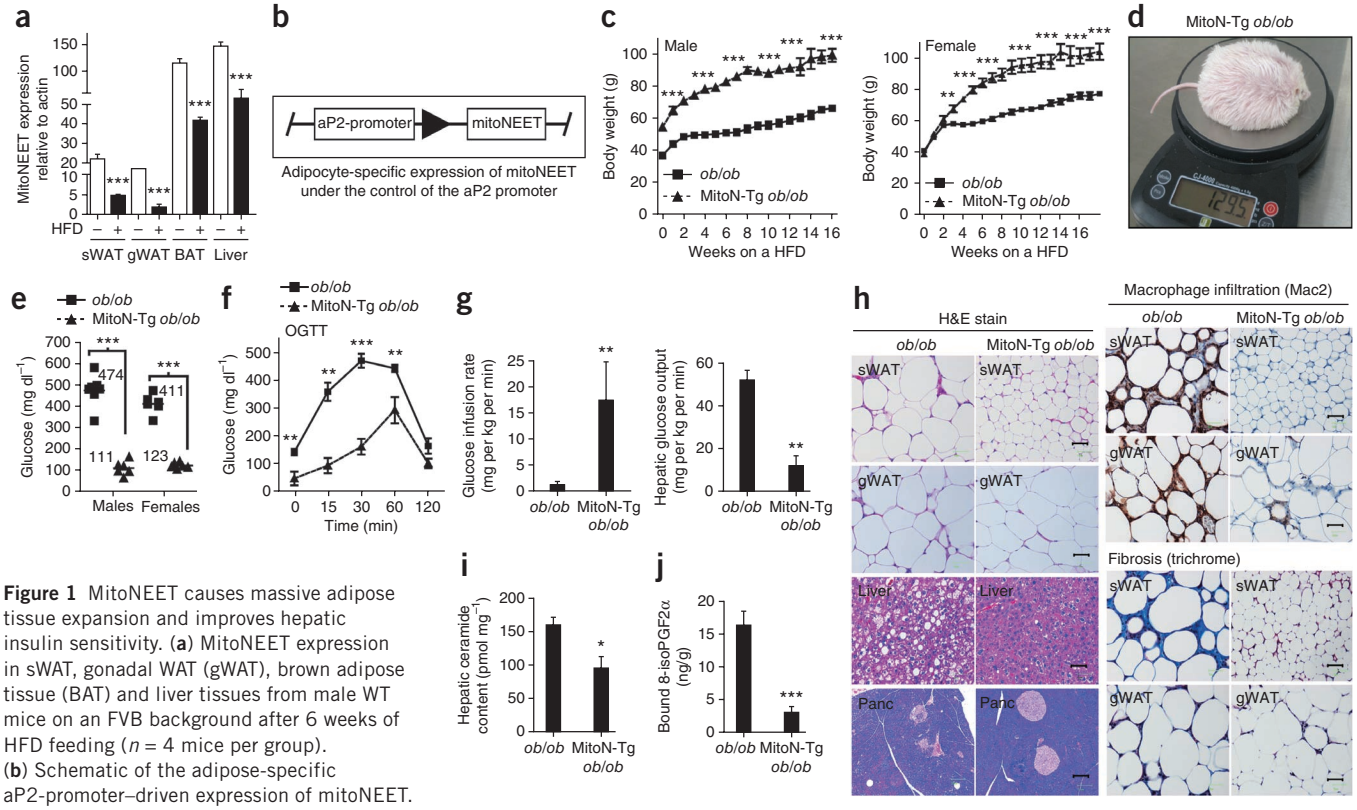

Figure 1 MitoNEET causes massive adipose tissue expansion and improves hepatic insulin sensitivity. (**a**) MitoNEET expression in sWAT, gonadal WAT (gWAT), brown adipose tissue (BAT) and liver tissues from male WT mice on an FVB background after 6 weeks of HFD feeding ($n = 4$ mice per group). (**b**) Schematic of the adipose-specific aP2-promoter–driven expression of mitoNEET. (**c**) Body weights during HFD feeding of male and female *ob/ob* mice on an FVB background (FVB *ob/ob* mice) and MitoN-Tg *ob/ob* mice ($n = 6$ per group). (**d**) A photograph of the heaviest HFD-challenged MitoN-Tg FVB *ob/ob* female mouse reported to date. (**e**) Fed-state systemic glucose concentrations during HFD feeding of FVB male and female *ob/ob* mice and male and female MitoN-Tg *ob/ob* mice ($n = 6$ per group). The values shown indicate the mean glucose concentrations for each group. (**f**) An OGTT (2.5 g per kg body weight, single gavage) of female FVB *ob/ob* and MitoN-Tg *ob/ob* mice ($n = 5$ mice per group). (**g**) Glucose infusion rates (left) and hepatic glucose output (right) during hyperinsulinemic-euglycemic clamp experiments performed on conscious unrestrained 10-week-old female FVB *ob/ob* mice and MitoN-Tg *ob/ob* mice ($n = 5$ mice per group). (**h**) H&E staining (left), macrophage infiltration (Mac2 immunohistochemistry) (top right) and fibrosis (trichrome stain) (bottom right) in sWAT, gWAT, liver and pancreas (Panc), as indicated, from chow-fed female FVB *ob/ob* mice and MitoN-Tg *ob/ob* mice. Scale bars, 50 μm; bottom left, 200 μm. (**i**) Hepatic ceramide content in female FVB *ob/ob* mice and MitoN-Tg *ob/ob* mice ($n = 4$ mice per group). (**j**) Lipid-induced (15 μl per g body weight of 20% intralipid, single gavage), ROS-promoted lipid damage (lipid peroxidation, as measured by the amount of bound 8-isoPGF2α, an isoprostane derived from arachidonic acid through *in vivo* lipid peroxidation that serves as a measure of oxidative stress) in FVB female *ob/ob* and MitoN-Tg *ob/ob* sWAT ($n = 5$ mice per group). $^*P < 0.05$, $^{**}P < 0.01$, $^{***}P < 0.001$ by Student's *t* test. All data shown are means ± s.e.m.

generate an adipose-specific transgenic mouse model of mitoNEET overexpression (MitoN-Tg mice) (**Fig. 1b**). This led to the overexpression of mitoNEET within a physiological range (approximately five-fold overexpression in sWAT, with lower expression in other fat pads). Notably, expression of the transgene was limited to the adipocytes and was not present in other cell types, including macrophages (data not shown).

To assess the extent to which mitoNEET action can affect adipose tissue expansion, we applied a more prolonged metabolic challenge. We wanted to determine how maintaining elevated expression of mitoNEET during adipose tissue expansion affects the cellular physiology of a mouse with a diabetic phenotype. We therefore generated *ob*/*ob* mice in a FVB background harboring the adipose-specific mitoNEET overexpression cassette. Both male and female MitoN-Tg *ob*/*ob* mice gained substantially more body weight than their nontransgenic *ob*/*ob* littermates (**Fig. 1c**), with the heaviest female MitoN-Tg *ob*/*ob* mouse having a body weight of 129.5 g (**Fig. 1d**). Despite their body weight, male and female MitoN-Tg *ob*/*ob* mice had euglycemic blood glucose concentrations, whereas their nontransgenic *ob*/*ob* counterparts had diabetic hyperglycemic concentrations (male *ob*/*ob* mice: 474 ± 26 mg dl^{-1} (mean ± s.e.m.); male MitoN-Tg *ob*/*ob* mice: 111 ± 14 mg dl^{-1}, $P < 0.001$; female *ob*/*ob* mice: 411 ± 19 mg dl^{-1}; female MitoN-Tg *ob*/*ob* mice: 123 ± 6 mg dl^{-1}, $P < 0.001$) (**Fig. 1e**). An oral glucose tolerance test (OGTT) on these morbidly obese transgenic mice revealed a profile that was comparable to that of fully glucose-tolerant wild-type (WT) mice despite using an oral glucose dose that was based on body weight (that is, the transgenic mice received a three to four times higher glucose load than the WT mice) (**Fig. 1f**). In hyperinsulinemic-euglycemic clamp studies, MitoN-Tg *ob*/*ob* mice required a significantly higher glucose infusion rate than nontransgenic *ob*/*ob* mice ($P < 0.01$, $n = 5$ mice per group) (**Fig. 1g**), implicating a higher whole-body insulin sensitivity in the transgenic mice. Hepatic insulin sensitivity was also enhanced in MitoN-Tg *ob*/*ob* mice, as shown by a markedly lower hepatic glucose output than nontransgenic *ob*/*ob* mice (**Fig. 1g**). Consistent with the improved carbohydrate metabolism, the histology of the liver, adipose tissue and pancreas were normalized in MitoN-Tg *ob*/*ob* mice compared to nontransgenic *ob*/*ob* mice, with negligible hepatic lipid accumulation (**Fig. 1h**). A normalization of adipocyte cell size was also apparent in the MitoN-Tg *ob*/*ob* mice, concomitant with limited sWAT immune-cell infiltration (**Fig. 1h**). Moreover, MitoN-Tg *ob*/*ob* mice retained the same number and morphology of islets as a WT mouse, whereas diabetic *ob*/*ob* mice retained less than half the number of islets of WT mice (WT: 32 ± 2 islets (mean ± s.e.m.); *ob*/*ob*: 14 ± 6 islets; MitoN-Tg *ob*/*ob*: 38 ± 2 islets). Furthermore, we found markedly less fibrosis in MitoN-Tg *ob*/*ob* mice than in their nontransgenic *ob*/*ob* counterparts, primarily evident in the sWAT, as determined by trichrome staining (**Fig. 1h**).

Ceramides are a group of sphingolipids that are frequently associated with insulin resistance[17]; consistent with this, MitoN-Tg *ob*/*ob* mice had significantly lower concentrations of hepatic ceramides than nontransgenic *ob*/*ob* mice ($P < 0.05$, $n = 4$ mice per group) (**Fig. 1i**). Similarly, diacylglycerols are another class of lipids that, when elevated in the liver, have been implicated in reduced cellular insulin responses[18]. Notably, MitoN-Tg *ob*/*ob* mice had markedly lower hepatic diacylglycerol concentrations than nontransgenic *ob*/*ob* mice (*ob*/*ob*: 1,644.9 ± 180.3 pmol mg^{-1} (mean ± s.e.m.); MitoN-Tg *ob*/*ob*: 936.8 ± 97.5 pmol mg^{-1}; $P < 0.05$), further suggesting an improved hepatic lipid profile.

After an oral gavage of 20% intralipid, we examined F2-isoprostane concentrations as a measure of reactive oxygen species (ROS)-driven lipid peroxidation[19]. Notably, MitoN-Tg *ob*/*ob* sWAT harbors markedly fewer ROS-induced lipid peroxidation products than *ob*/*ob* sWAT (**Fig. 1j**), showing a paradoxical low degree of oxidative stress in a morbidly obese setting. We found similar results in MitoN-Tg mice exposed to HFD in the absence of the *ob*/*ob* mutation (data not shown). In addition, we were able to initiate similar fat-pad expansion by directly infecting the sWAT of WT mice with a mitoNEET-expressing adeno-associated virus (AAV), which prompted a local threefold overexpression of mitoNEET compared to injection of a control virus into the collateral fat pad (data not shown). Collectively, these data indicate that overexpression of mitoNEET can promote adipose tissue expansion under multiple different conditions, such as HFD and loss of leptin expression, using various approaches for overexpression.

MitoNEET-enhanced lipid uptake and adiponectin production

Younger mice carrying the mitoNEET transgene in a WT background that are maintained on a chow diet have no considerable differences in body weight or insulin sensitivity when compared to WT mice (data not shown). We proposed that an unchallenged setting would be an ideal condition to evaluate the MitoN-Tg sWAT gene expression profile in more detail, as we would not have the additional confounders of chronic obesity and insulin resistance, which alter the microarray profile secondary to the initial transcriptional changes. The main transcriptional fingerprints that were substantially altered in sWAT by mitoNEET overexpression are listed in **Supplementary Table 1**. The gene regulatory pathways that were markedly altered in response to mitoNEET induction were adipogenesis, triglyceride synthesis, nonesterified fatty acid re-esterification, fatty acid biosynthesis, lipid-droplet–associated protein synthesis, fatty acid uptake, fatty acid transport and glucose uptake (**Supplementary Table 1**); we confirmed these changes using RT-PCR analysis (**Fig. 2a** and **Supplementary Fig. 1**). **Supplementary Table 2** shows a list of the RT-PCR primer sequences of differentially expressed genes that we identified in the microarray cluster analysis of sWAT derived from WT and MitoN-Tg mice. Notably, we found a marked upregulation of the fatty acid transporter protein Cd36 in MitoN-Tg sWAT when compared with WT sWAT, suggesting that mitoNEET action may alter the kinetics of cellular lipid uptake. Indeed, a triglyceride clearance test revealed a striking efficacy in the rate of lipid clearance in MitoN-Tg mice. Although the WT mice had the expected hyperlipidemic excursion of triglyceride after exposure to an oral lipid gavage, MitoN-Tg mice had a significantly higher rate of triglyceride clearance ($P < 0.01$, $n = 6$ mice per group) (**Fig. 2b**).

The ability of MitoN-Tg mice to rapidly dispose of exogenous lipids, coupled with the long-term ability to enhance fat-mass expansion, is a phenotype reminiscent of that of adiponectin-overexpressing mice[5]. The transcriptional upregulation of adiponectin that we observed in the MitoN-Tg mice (**Fig. 2a**) is consistent with a potential involvement of adiponectin in the upregulation process of enhanced lipid storage in adipocytes. Indeed, MitoN-Tg mice had markedly higher circulating concentrations of adiponectin than WT mice (**Supplementary Table 3**), with a prominently higher amount of the high–molecular-weight form of adiponectin (data not shown), highlighting the ability of mitoNEET to exert a constitutive stimulatory effect on adiponectin production and release. A similar effect on adiponectin upregulation is also observed in MitoN-Tg *ob*/*ob* mice when compared with nontransgenic *ob*/*ob* mice (**Supplementary Table 4**). The marked upregulation of adiponectin protein expression (**Fig. 2c**) was only evident in transgenic sWAT and was not apparent

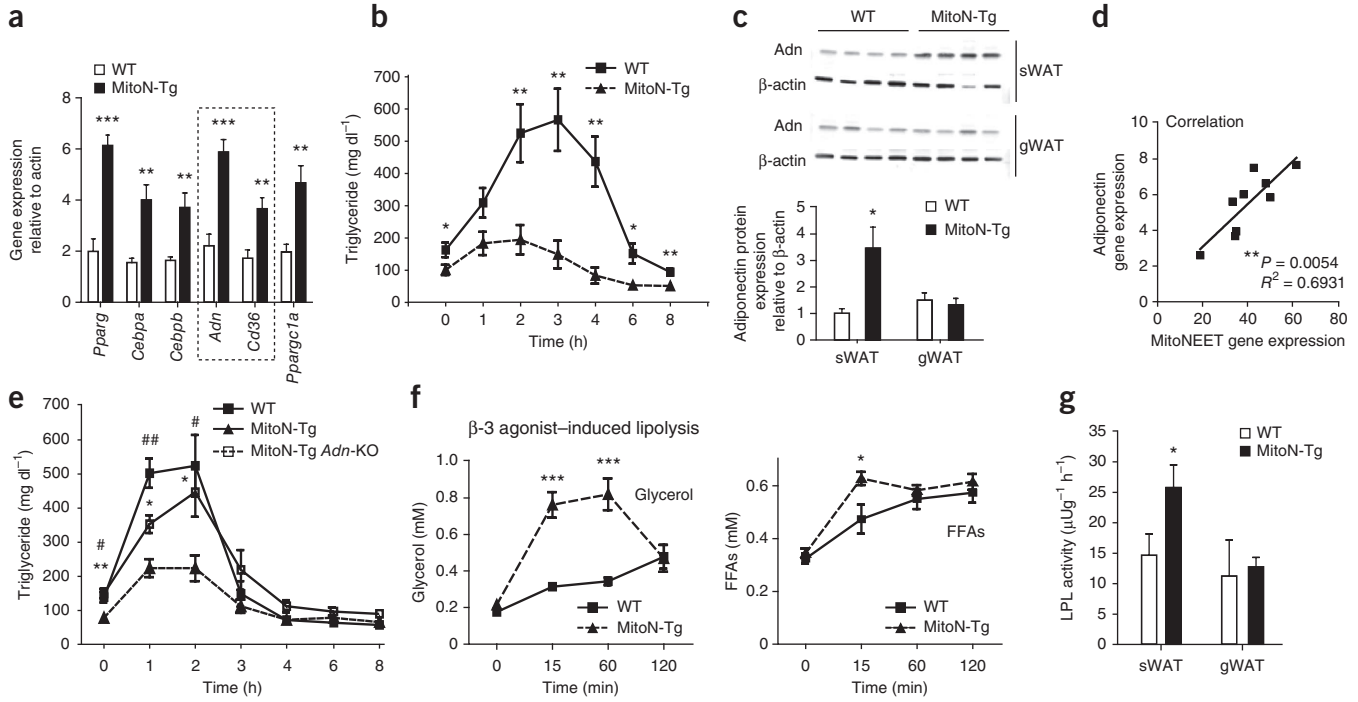

Figure 2 MitoNEET promotes lipid uptake by stimulating adiponectin production and heightening β-3 adrenergic agonist sensitivity. (**a**) RT-PCR showing gene expressions of key microarray hits from male FVB WT and MitoN-Tg sWAT ($n = 9$ sWAT samples per group). The dashed box highlights the crucial changes observed for adiponectin and Cd36. (**b**) Triglyceride clearance test (20% intralipid, 15 μl per g body weight, single gavage) in male FVB WT and MitoN-Tg mice ($n = 6$ mice per group). (**c**) Western blot showing adiponectin expression in WT and MitoN-Tg sWAT and gWAT fat pads ($n = 4$ mice per group). (**d**) The correlation between mitoNEET transgene expression and endogenous adiponectin expression in MitoN-Tg sWAT ($n = 9$ per group). (**e**) Triglyceride clearance test (20% intralipid, 15 μl per g body weight, single gavage) in male FVB WT mice, MitoN-Tg mice and MitoN-Tg adiponectin knockout (*Adn*-KO) mice ($n = 6$ mice per group). $^{*}P < 0.05$, $^{**}P < 0.01$ correspond to comparisons between WT mice and MitoN-Tg mice. $^{\#}P < 0.05$, $^{\#\#}P < 0.01$ correspond to comparisons between WT mice and *Adn*-KO MitoN-Tg mice. A Student's *t* test or a two-way analysis of variance was used to calculate *P* values. (**f**) Circulating glycerol (left) and FFA concentrations (right) in male FVB WT and MitoN-Tg mice during a β-3 adrenergic agonist sensitivity test (1 mg per kg body weight) CL316,243 intraperitoneally, $n = 7$ mice per group). (**g**) LPL activity in WT and MitoN-Tg sWAT and gWAT ($n = 5$ mice per group). $^{*}P < 0.05$, $^{**}P < 0.01$, $^{***}P < 0.001$. A Student's *t* test was used to determine *P* values. All data are means ± s.e.m.

in gonadal WAT (gWAT), suggesting that local mitoNEET levels within a fat pad govern adiponectin production. Indeed, we found that adiponectin expression showed a tight positive correlation with how much mitoNEET was expressed within a given fat pad (**Fig. 2d**). Given this result, we examined whether mitoNEET-enhanced lipid clearance is mediated directly through adiponectin upregulation. MitoN-Tg adiponectin knockout mice had significantly lower rates of triglyceride clearance than MitoN-Tg mice ($P < 0.05$, $n = 6$ mice per group) (**Fig. 2e**), suggesting that augmented lipid uptake is at least partially dependent on a mitoNEET-adiponectin axis.

Whereas no differences were apparent between WT mice and MitoN-Tg mice in terms of systemic glucose and insulin concentrations under chow-fed conditions (**Supplementary Table 3**), we did find elevated systemic FFA and glycerol concentrations in MitoN-Tg mice after fasting them for 24 h (**Supplementary Table 3**), suggesting that mitoNEET concentration in adipocytes may influence fasting-induced lipolysis. In response to extracellular stimuli by catecholamines, adipocytes hydrolyze stored neutral triglycerides to liberate FFAs and glycerol[20]. Notably, after stimulation with β-3 adrenergic agonist, MitoN-Tg mice released considerably more glycerol than WT mice (**Fig. 2f**), a phenotype also similar to that of adiponectin transgenic mice[21]. However, FFA release is massively substoichiometric to glycerol release. Thus, whereas we theoretically expected 3 moles of FFA to be released for every mole of glycerol released (a ratio that is usually closer to 2:1 in WT mice), we found less than 0.3 moles of FFAs liberated per mole of glycerol in the transgenic mice. This suggests that an extremely efficient re-esterification of FFAs to triglyceride occurs in these mice, along with an excess local pool of glycerol. Such a phenomenon is particularly apparent in an *ob*/*ob* setting, where the profound reduction in FFA efflux becomes problematic after fasting, a condition under which glucose concentrations rapidly achieve hypoglycemic levels (data not shown).

Phosphoenolpyruvate carboxykinase (Pepck) has a pertinent role in maintaining the homeostasis of FFA re-esterification in adipose tissue[22], particularly through glyceroneogenesis[23]. The marked upregulation in Pepck expression in MitoN-Tg sWAT (**Supplementary Fig. 1**) suggests a mitoNEET-induced Pepck-dependent stimulation of glyceroneogenic pathways, which may effectively promote FFA re-esterification into the triglyceride pool within adipocytes. In addition, β-3 adrenergic stimulation of WAT is known to trigger the rapid release of insulin from pancreatic β cells[19]. After injection of the β-3 adrenoceptor agonist, we found a sharp rise in insulin concentrations accompanied by severe hypoglycemia in transgenic mice (data not shown), suggesting a fully functional and highly active adipo-insular axis in transgenic mice.

Lipoprotein lipase (LPL) has a key role in the clearance of circulating triglycerides and their routing toward either storage or oxidative tissues. MitoN-Tg sWAT has significantly more local LPL activity than WT sWAT (WT sWAT: 14.6 ± 3.5 $\mu Ug^{-1}\ h^{-1}$ (mean ± s.e.m.); MitoN-Tg sWAT: 25.7 ± 3.7 $\mu Ug^{-1}\ h^{-1}$; $P < 0.001$), with no

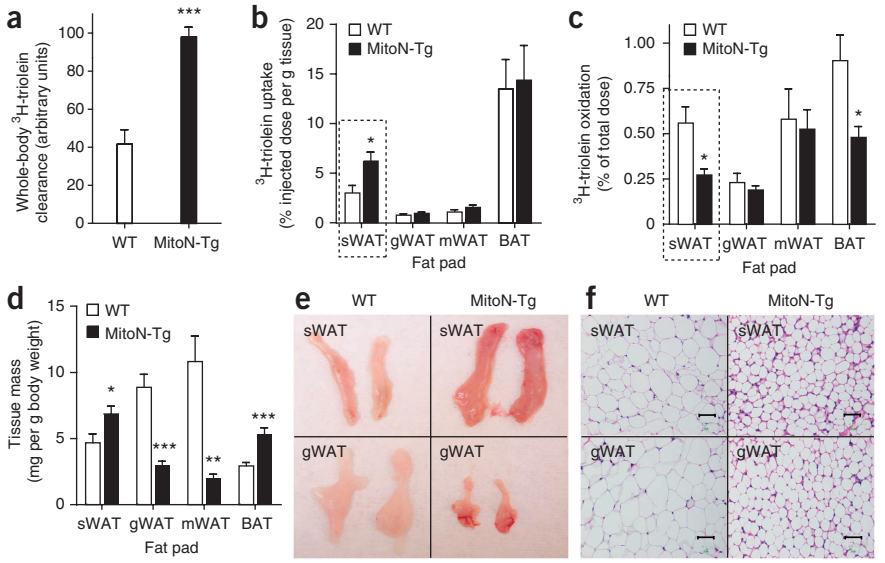

Figure 3 MitoNEET-induced alterations in fatty acid metabolism. (**a**) Whole-body ^{3}H-triolein lipid clearance in male FVB WT and MitoN-Tg mice at 15 min after injection (2 μCi per mouse in 100 μl of 5% intralipid, single tail-vein injection) ($n = 6$ mice per group). (**b**–**d**) ^{3}H-triolein lipid-uptake (**b**), β-oxidation (**c**) and tissue mass (**d**) in sWAT, gWAT, mWAT and BAT fat pads of WT and MitoN-Tg mice ($n = 6$ samples per group). Dashed boxes highlight the fat pad primarily overexpressing mitoNEET. (**e**,**f**) A representative photograph (**e**) and H&E staining (**f**) of sWAT and gWAT fat pads from a WT and a MitoN-Tg mouse. $^*P < 0.05$, $^{**}P < 0.01$, $^{***}P < 0.001$ by Student's t test. Scale bars, 50 μm. All data are means ± s.e.m.

differences in local LPL activity between MitoN-Tg and WT gWAT fat pads (**Fig. 2g**). These data indicate an exceptionally responsive subcutaneous fat pad in the transgenic mice, a phenotype that is crucially dependent on, and directly proportional to, the local overexpression of mitoNEET.

MitoNEET-mediated effects on fatty acid metabolism

To further tie mitoNEET expression to fatty acid metabolism, we injected a ^{3}H-triolein tracer into MitoN-Tg mice and WT mice to quantitatively assess lipid storage and β-oxidation rates. We found that MitoN-Tg mice had a significantly higher (235%; $P < 0.001$) rate of whole-body ^{3}H-triolein clearance than WT mice (**Fig. 3a**), with sWAT being primarily responsible for the bulk of the differential (**Fig. 3b**) of all the tissues examined (**Supplementary Fig. 2a**). Considering that sWAT is the primary site of mitoNEET overexpression, the higher expression of mitoNEET locally within subcutaneous adipocytes is probably the direct mediator of these effects on lipid clearance. In parallel, we noted markedly lower β-oxidation rates in MitoN-Tg than WT sWAT and brown adipose tissue (BAT) (BAT being a secondary site of mitoNEET overexpression) (**Fig. 3c** and **Supplementary Fig. 2b**). Quantitatively, MitoN-Tg sWAT and BAT were substantially larger than WT sWAT and BAT (**Fig. 3d**), consistent with a tight link to local overexpression of mitoNEET within these fat pads. Visually, MitoN-Tg sWAT appeared darker in color than WT sWAT (**Fig. 3e**). Conversely, and presumably compensatory to sWAT hyperproliferation, MitoN-Tg gWAT and mesenteric WAT (mWAT) fat pads were markedly smaller than WT gWAT and mWAT fat pads (**Fig. 3d**,**e** and **Supplementary Fig. 2c**). These observations suggest that by manipulating mitoNEET expression differentially in various fat pads, we can disrupt the steady-state distribution of lipid storage, thereby preferentially redistributing lipids toward fat pads enriched for mitoNEET.

A qualitative histological examination of adipose tissue revealed that the adipocytes are smaller in MitoN-Tg sWAT than in WT sWAT (**Fig. 3f**), indicating that within a mitoNEET-enriched environment, healthy adipose tissue expansion through adipocyte hyperplasia prevails rather than the metabolically unfavorable adipocyte hypertrophic expansion that is typically observed in states of obesity-associated insulin resistance[24]. In addition, MitoN-Tg gWAT adipocytes are smaller than WT gWAT adipocytes (**Fig. 3f**), suggesting a diversion of lipids away from this fat pad to avoid formation of hypertrophic adipocytes.

MitoNEET modulates mitochondrial function and iron content

Previous reports have established mitoNEET as an outer mitochondrial membrane protein. Although the phenotypic changes associated with the alteration of mitoNEET expression are robust, the question arises of how an outer mitochondrial membrane protein exerts such profound effects on β-oxidation rates. MitoNEET can serve as an iron-sulfur–cluster transfer protein[25]; however, the physiological relevance of these clusters is unknown—they may have a role in mitochondrial iron metabolism. Indeed, we found that mitoNEET overexpression at the level of the mitochondrion results in an adipocyte mitochondrial iron metabolism that is markedly out of balance. More specifically, MitoN-Tg sWAT mitochondria contain significantly lower concentrations of iron than WT sWAT mitochondria ($P < 0.001$, $n = 7$ sWAT per group) (**Fig. 4a**). This almost 50% lower concentration of mitochondrial iron suggests a crucial involvement of mitoNEET in supplying the components of the ETC with iron, a rate-limiting component for ETC activity[26]. Furthermore, we noted markedly lower heme iron concentrations in MitoN-Tg than WT sWAT mitochondria (data not shown); as mitochondrial heme synthesis and iron-sulfur–cluster metabolism are tightly linked processes[27], this further highlights mitoNEET-induced alterations in iron homeostasis. Moreover, when assessing either WT mice fed a high-iron diet or mice with hemochromatosis (induced with targeted deletion of the *Hfe* gene, which leads to defects in iron handling and a cellular iron overload)[28], we found that the total expression of mitoNEET was considerably upregulated (**Fig. 4b**) in both groups, with a notable stabilization of an SDS-resistant mitoNEET dimer. These results could be consistent with a counter-regulatory upregulation of mitoNEET under conditions of excess iron in an attempt to curb the additional transport of iron into the mitochondrial matrix under conditions of iron overload.

To address how mitoNEET lowers β-oxidation and promotes lipid accumulation, we examined the adipocyte overexpression model further. When examining the mitochondrial membrane potential ($\Delta\Psi m$), 3T3-L1 preadipocytes stably transfected with either high or low concentrations of mitoNEET had a low $\Delta\Psi m$ compared to cells transfected with a control plasmid (**Fig. 4c**); a similar reduction in $\Delta\Psi m$ occurred as a result of treatment with TZD (**Fig. 4c**). This mitoNEET-induced reduction in $\Delta\Psi m$ may reflect insufficient ETC activity[29], inefficient substrate supply to the mitochondria or an increased proton flux back into the

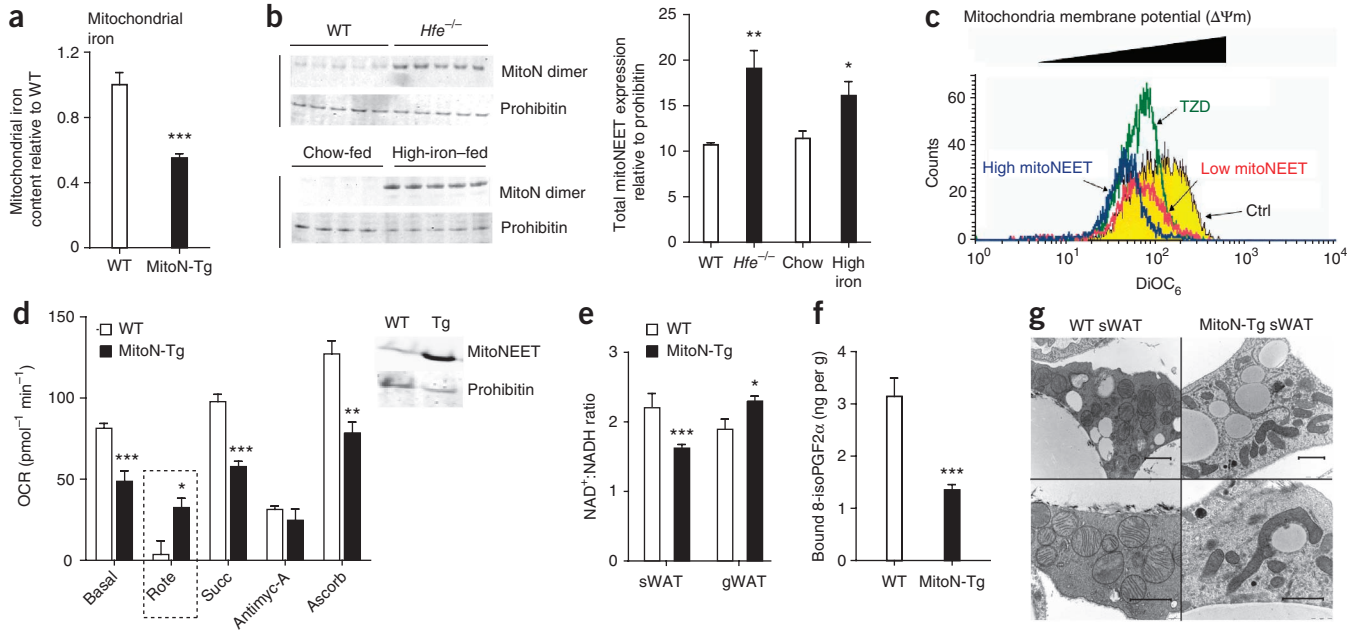

Figure 4 MitoNEET compromises mitochondrial dynamics and morphology by modulating mitochondrial iron content. (**a**) Mitochondrial iron content in WT and MitoN-Tg sWAT ($n = 7$ samples per group). (**b**) Total mitoNEET expression (monomer and dimer) in WT and *Hfe*$^{-/-}$ mice (top) and in control mice fed a chow diet and mice fed a high-iron diet ($n = 5$ mice per group). (**c**) Mitochondrial membrane potential ($\Delta\Psi$m) determined using 3,3′-dihexyloxacarbocyanine iodide ($DiOC_6$) incubated with control (vehicle) or 3T3-L1 preadipocytes with either low or high expression of mitoNEET. Yellow panel, control (vehicle); green panel, TZD treatment; red panel, low mitoNEET expression; blue panel, high mitoNEET expression. (**d**) OCRs in mitochondria (1 μg) isolated from WT and MitoN-Tg sWAT in response to sequential additions of DMEM (basal conditions, containing FCCP and the substrates pyruvate and malate), rotenone (Rote, complex I inhibitor), succinate (Succ, complex II substrate), antimycin-A (Antimyc-A, complex III inhibitor), ascorbate (Ascorb) and tetramethylphenylenediamine (TMPD, cytochrome *c* substrate) ($n = 4$ samples per group). The dashed box emphasizes the key changes observed in OCRs between WT sWAT and MitoN-Tg sWAT in response to rotenone (discussed in the Results section). Prohibitin was used as a mitochondrial protein loading control. (**e**) NAD^+:NADH ratio in WT and MitoN-Tg sWAT and gWAT ($n = 5$ mice per group). (**f**) Lipid-induced (15 μl per g body weight of 20% intralipid, single gavage with tissues harvested after a 6-h induction), ROS-promoted lipid damage (lipid peroxidation, as measured by the amount of bound 8-isoPGF2α) in WT and MitoN-Tg sWAT ($n = 5$ mice per group). (**g**) Representative electron microscopy images (16,500× and 26,500× magnifications) of unchallenged WT and MitoN-Tg sWAT. $^*P < 0.05$, $^{**}P < 0.01$, $^{***}P < 0.001$ by Student's *t* test. Scale bars, 1 μm. All data are means ± s.e.m.

mitochondrial matrix, all of which are a direct consequence of a local elevation in mitoNEET expression.

To directly establish whether mitoNEET alters ETC activity, we performed electron-flow analyses and assessed oxygen-consumption rates (OCRs), a method that was previously established to assess mitochondrial function[30]. Of note, such OCR measurements are performed in the presence of the chemical uncoupler carbonyl cyanide 4 (trifluoromethoxy)phenylhydrazone (FCCP). MitoN-Tg sWAT mitochondria have markedly lower OCRs in response to the substrates pyruvate, malate, succinate and ascorbate than do WT sWAT mitochondria (**Fig. 4d**). However, MitoN-Tg sWAT mitochondria have markedly higher OCRs in response to the complex I inhibitor rotenone (**Fig. 4d**). Rotenone can promote ROS-induced oxidative stress[31]; therefore, an ineffective inhibition of complex I by rotenone in MitoN-Tg mitochondria suggests that an indirect interference by mitoNEET may minimize ROS-driven damage. Moreover, we found that MitoN-Tg sWAT has a significantly lower ratio of NAD^+ to NADH than WT sWAT ($P < 0.001$, $n = 5$) (**Fig. 4e**). This build-up of reduced NADH equivalents in MitoN-Tg sWAT suggests that NADH is insufficiently reoxidized by the ETC or that mitoNEET may enhance glycolytic rates (an NADH-generating process) to compensate for reduced β-oxidation. Notably, in parallel with the low OCRs in MitoN-Tg sWAT, we found concomitant higher glycolytic rates in MitoN-Tg compared to WT whole-tissue sWAT slices (as judged by a higher extracellular acidification rate (ECAR), an established indicator of glycolysis[32]) (**Supplementary Fig. 3**). This high amount of glycolytic flux supports a model of a mitoNEET-driven shift in substrate utilization and metabolism from lipid-based substrates to carbohydrate-based substrates.

Defects in ETC activity have a marked impact on ROS production[31,33]. After an oral gavage of 20% intralipid to create an environment of heightened lipid-stimulated ROS production within MitoN-Tg and WT sWAT, we assessed F2-isoprostane concentrations to gauge ROS-driven lipid peroxidation[19]. Notably, MitoN-Tg sWAT harbored substantially fewer products of ROS-induced lipid peroxidation than did WT sWAT (**Fig. 4f**). Low ROS concentrations in mitoNEET-enriched fat pads are therefore a characteristic feature of mitoNEET-overexpressing adipocytes. To complement these biochemical assays, we focused on mitochondrial morphology. Electron microscopy analyses revealed that MitoN-Tg sWAT mitochondria are elongated and form long filamentous structures (**Fig. 4g**). Moreover, these mitochondria are recurrently juxtaposed to lipid-droplet–like structures (**Fig. 4g**), a phenomenon that has been observed in exercising skeletal-muscle mitochondria in response to increasing energy demand[34]. More mitochondria are visible per section of adipose tissue in MitoN-Tg than WT sWAT (**Fig. 4g**), suggesting induction of mitochondrial biogenesis. The markedly higher peroxisome proliferator-activated-γ coactivator 1-α (Pgc1-α) message levels in MitoN-Tg than WT sWAT (**Fig. 2a**), a key regulator of mitochondrial biogenesis[35], is consistent with this observation.

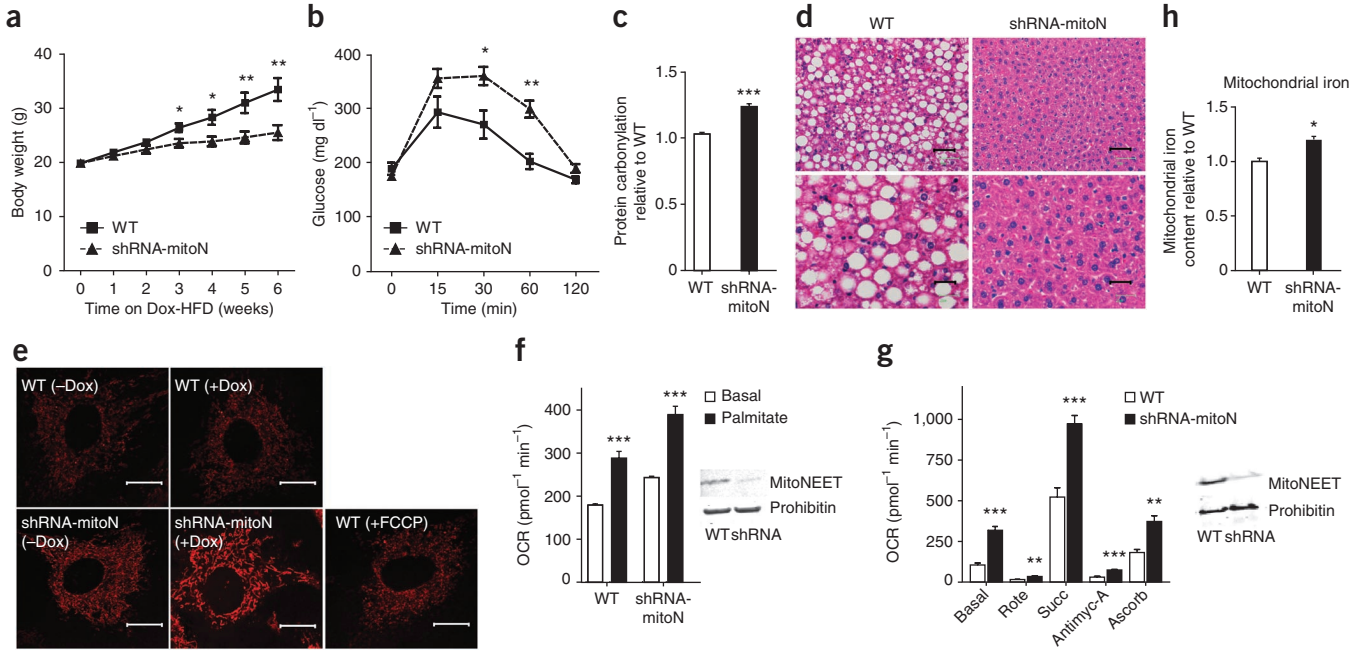

Figure 5 A lack of mitoNEET enhances mitochondrial oxidative capacity. (**a**) Gain in body weight of male C57/BL6 WT and shRNA-mitoN mice during Dox-HFD feeding ($n = 5$ mice per group). (**b**) An OGTT (2.5 g per kg body weight, single gavage) of male C57/BL6 WT and shRNA-mitoN mice after Dox-HFD feeding ($n = 5$ mice per group). (**c**) Hepatic ROS-induced protein damage (protein carbonylation) in male C57/BL6 WT and shRNA-mitoN mice after Dox-HFD feeding ($n = 5$ mice per group). (**d**) Representative H&E staining of WT and shRNA-MitoN livers after Dox-HFD feeding. Scale bars, top, 50 μm; bottom 25 μm. (**e**) TMRM-treated WT and shRNA-MitoN MEFs (with or without Dox treatment) to assess $\Delta\Psi m$. The chemical uncoupler FCCP was used as an additional control. All images were taken by confocal microscopy at 63× magnification. Scale bars, 20 μm. (**f**) OCRs in Dox-treated WT MEFs and shRNA-MitoN MEFs in response to basal conditions (low glucose) followed by the addition of palmitate and then etomoxir (an inhibitor of lipid oxidation) ($n = 10$ mice per group). (**g**) OCRs for mitochondria (5 μg) isolated from liver tissues of Dox-chow–fed WT and shRNA-MitoN mice in response to sequential additions of DMEM (basal conditions, containing FCCP and the substrates pyruvate and malate), rotenone (Rote), succinate (Succ), antimycin-A (Antimyc-A), ascorbate (Ascorb) and TMPD ($n = 4$ samples per group). Prohibitin was used as a mitochondrial protein loading control. (**h**) Mitochondrial iron content in WT and shRNA-mitoN livers ($n = 7$ samples per group). $^*P < 0.05$, $^{**}P < 0.01$, $^{***}P < 0.001$ by Student's *t* test. All data are means ± s.e.m.

Liver-specific overexpression of mitoNEET

To examine an alternative, acute *in vivo* modality to induce mitoNEET overexpression in cells other than adipocytes, we generated a mouse, termed here the TRE-mitoNEET mouse (TRE-mitoN), in which the expression of mitoNEET was driven by a tetracycline-inducible promoter element (a tet-responsive element, or TRE). For this promoter element to be operational, the presence of the 'tet-on' transcription factor, rtTA, is required. We provided this factor in a hepatocyte-specific manner through a mouse that harbors the rtTA component under the control of a ubiquitously active Rosa26 promoter; a transcriptional stop cassette flanked by two *loxP* sites prevents transcription of the rtTA gene. We activated hepatic expression with an albumin-promoter–driven Cre transgene.

We achieved hepatocyte-specific, doxycycline (Dox)-inducible mitoNEET overexpression by exposing the TRE-mitoN mice to an albumin-promoter–driven Cre recombinase (**Supplementary Fig. 4a**). After feeding mice Dox containing HFD (Dox-HFD), they attained a substantial and reliable threefold overexpression of mitoNEET protein (**Supplementary Fig. 4b**). Using this method, we were able to show the usefulness of mitoNEET as a manipulator of mitochondrial activity in other cell types. Consistent with our model of mitoNEET overexpression in adipose tissue, a mitoNEET-driven augmentation in lipid storage was preserved in the livers of TRE-mitoN mice. Qualitatively, hepatic lipid droplets were more prevalent in TRE-mitoN mice than in WT mice (**Supplementary Fig. 4c**); this reflects a decline in mitochondrial respiratory capacity in the former group (**Supplementary Fig. 4d**). Collectively, this suggests a similar effect exerted by mitoNEET in a cell type that is distinct from adipocytes, indicating a common effect of mitoNEET on cellular physiology in different tissue types.

Diametrically opposed effects for lower mitoNEET expression

MitoNEET overexpression allowed us to effectively manipulate mitochondrial function. To examine whether we could manipulate mitochondrial activity in an opposite direction through a reduction in mitoNEET expression, we generated mice harboring a Dox-inducible shRNA knockdown construct for mitoNEET (shRNA-mitoN mice) (**Supplementary Fig. 5a**); this construct was effective in a majority of tissues, including adipose tissue and the liver (data not shown), thus creating a systemic inducible knockdown of mitoNEET. After feeding shRNA-mitoN mice a chow diet containing Dox (Dox-chow), we found a marked reduction in the amount of mitoNEET protein in their adipose tissue and liver (**Supplementary Fig. 5b**), which are the two tissues we opted to focus on in our analysis. Initial observations revealed that during Dox-HFD feeding, shRNA-mitoN mice gained considerably less body weight than WT littermates (**Fig. 5a**). Notably, despite having lower body weights, shRNA-mitoN mice had worse glucose tolerance than WT littermates (**Fig. 5b**). Given that we effectively modulated the ETC with mitoNEET overexpression, we hypothesized that this deterioration in insulin sensitivity may arise from an intensified amount of oxidative-stress[33,36]. Indeed, shRNA-mitoN mice harbored a high degree of hepatic ROS-induced

protein damage (**Fig. 5c**), as assessed by enhanced amounts of protein carbonylation, a measure that was previously established to gauge oxidative damage within a cell[37]. Consistent with this, antioxidant treatment of WT and shRNA-mitoN mouse embryonic fibroblasts (MEFs) or primary hepatocytes isolated from WT and shRNA-mitoN mice was able to reverse a palmitate-induced reduction in the amount of phosphorylated Akt (pAkt) (**Supplementary Fig. 5c**), suggesting that the ROS-associated worsening in glucose tolerance may be alleviated through the use of antioxidant treatments to reverse the negative effect on insulin signaling.

A histological examination of livers after Dox-HFD feeding revealed that shRNA-mitoN mice have less lipid accumulation in their livers than do WT mice (**Fig. 5d**), suggesting a local augmentation in β-oxidation. When examining the $\Delta\Psi m$, we found substantially enhanced tetramethylrhodamine methyl ester (TMRM) staining in Dox-induced shRNA-mitoN MEFs compared to WT MEFs treated with or without Dox (**Fig. 5e**). In terms of mitochondrial oxidative capacity, shRNA-mitoN MEFs had significantly higher OCRs in response to palmitate than did WT MEFs ($P < 0.001$, $n = 10$) (**Fig. 5f**), directly showing that a reduction in mitoNEET expression enhances β-oxidation. When assessing electron flow, hepatic mitochondria isolated from Dox-chow–fed shRNA-mitoN mice had markedly higher OCRs in response to pyruvate, malate, succinate and ascorbate than hepatic mitochondria from WT mice on the same diet (**Fig. 5g**), indicating higher mitochondrial activity in the absence of mitoNEET regardless of the substrate source. In light of this result, a previous report that included a partial characterization of cardiac mitochondria isolated from a systemic constitutive mitoNEET knockout mouse showed reduced oxidative capacity[13]. It is unclear what leads to these differential effects; however, it is probable that the tissues used in these latter studies, which develop in the constitutive absence of mitoNEET, may have compensatory mechanisms that prevail under the assay conditions used.

All the readouts from our loss-of-function mice were diametrically opposed to the gain-of-function phenotypes that we found in the first part of the analysis. This suggests that there may be a similar underlying mechanism that affects mitochondrial activity over the entire range of differential mitoNEET expressions. In addition, we observed higher concentrations of mitochondrial iron with a low expression of mitoNEET in the shRNA-mitoN mice compared to WT mice (**Fig. 5h**), consistent with a role of mitoNEET as a key factor in the regulation of mitochondrial iron content.

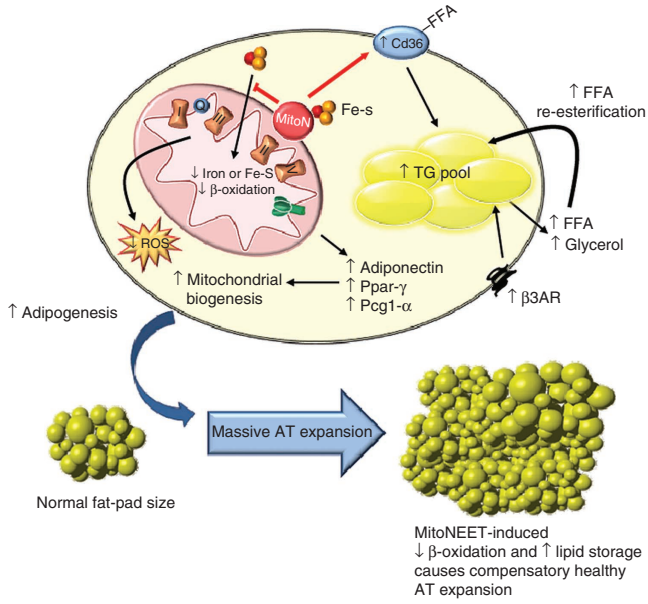

Figure 6 Proposed mechanism of mitoNEET action. Schematic representation of the intracellular involvement of mitoNEET in adipocyte physiology based on its ability to manipulate mitochondrial function. There are system-wide metabolic consequences arising from a mitoNEET-induced mitochondrial perturbation at the level of the adipocyte. MitoNEET affects mitochondrial iron content, which may contribute to the decline in β-oxidation, and enhances fatty acid uptake by signaling through Cd36. Compromised mitochondrial function therefore triggers a compensatory upregulation of adipogenesis, β-3 adrenergic signaling and mitochondrial biogenesis. The cellular decrease in mitochondrial activity further enhances lipid influx into the cell. The inability to use these lipids effectively in the mitochondria shunts surplus substrates into the triglyceride (TG) pool. Consequently, low β-oxidation rates, high Ppar-γ activity and increased adiponectin levels accompanied by excess lipid storage results in gross adipose tissue (AT) expansion. The ability to store massive amounts of lipids in the sWAT results in a highly beneficial system-wide improvement in whole-body insulin sensitivity with minimized lipotoxic effects in other tissues. β3AR, the receptor for the catecholamines.

DISCUSSION

We have developed a new tool to specifically alter the amount of mitochondrial activity in adipocytes and hepatocytes. We took advantage of the properties of the mitochondrial protein mitoNEET, which allowed us to profoundly alter mitochondrial function and lipid homeostasis in a cell-type–specific manner, thereby altering whole-body insulin sensitivity. We found these effects in a complementary set of mouse models that involve multiple independent approaches to achieve alterations in mitoNEET expression within a physiological range. We used an adipose-specific transgenic model, an inducible tissue-specific overexpression system and an inducible constitutive knockdown of mitoNEET. The overexpression of mitoNEET allowed us to compromise mitochondrial function to disrupt the cellular energy balance, driving a decline in β-oxidation and causing a compensatory enhancement in cellular nutrient uptake. This triggered chronic adipose tissue expansion, and the mice in this model grew massively obese to a weight that was on par with, or substantially higher than, the maximum weight reported in the literature for *Mus musculus*. Despite their obesity, mitoNEET overexpression during high caloric intake resulted in system-wide improvements in insulin sensitivity, thereby providing a model of a metabolically healthy, obese state that minimizes lipotoxicity in tissues that are prone to store lipids during excess caloric intake (**Fig. 6**), a phenomenon that is also observed clinically[38]. We focused our analysis primarily on adipose tissue; however, an upregulation and knockdown of mitoNEET causes profound mitochondrial alterations in hepatocytes, MEFs and 3T3-L1 fibroblasts, suggesting that the observations in adipocytes may apply to other cell types as well. Future assessments should reveal more systematically which cell types are particularly prone to regulation by mitoNEET and under what physiological conditions this regulation may be relevant. This may be a function of how much 'spare capacity' mitochondria have under a given physiological condition; in other words, whether they operate at a near maximal rate relative to the completely uncoupled state. It is likely that such mitochondria would be more markedly affected by subtle changes in mitochondrial iron metabolism.

Ectopic lipid accumulation is a major risk factor in the progression of insulin resistance[39]. Our mice with adipocyte-specific overexpression of mitoNEET have only minimal amounts of ectopic lipids, thereby preserving insulin sensitivity despite excess caloric intake.

The mechanisms for partitioning lipid storage versus β-oxidation are not fully defined, particularly in the context of the adipocyte. A key phenotype in transgenic mice is their enhanced lipid uptake and storage into sWAT, suggesting that mitoNEET may contribute to adjusting the relative ratio of energy stored to energy burned by altering mitochondrial bioenergetics. Another key finding was that manipulation of β-oxidation at the level of the white adipocyte causes a profound net systemic contribution toward whole-body energy homeostasis. In our model, incomplete β-oxidation may increase the cellular pool of peroxisome proliferator-activated receptor γ (Ppar-γ) ligands. Both high amounts of Ppar-γ and increased adipogenesis in the transgenic setting are consistent with this possibility.

Adiponectin is a 30-kDa protein secreted exclusively from adipocytes that exerts antidiabetic, anti-inflammatory and antiatherogenic properties[6,7]. Adequate mitochondrial function and biogenesis are crucial determinants for the folding and secretion of adiponectin[40–42]; therefore, one of our aims was to establish and strengthen the evidence for this relationship. Indeed, mitoNEET overexpression causes a substantial increase in the amount of adiponectin, both transcriptionally and post-transcriptionally in transgenic sWAT, prompting an increase in circulating adiponectin concentrations. This upregulation of adiponectin may also be central to the enhanced triglyceride clearance in mitoNEET transgenic mice, as this effect was blunted when we crossed mitoNEET-overexpressing mice into an adiponectin-null background. Taken together, the adipocyte-specific impairment in β-oxidation led to a substantial local increase in adiponectin production and release; this may be a valuable observation in the context of our teleological understanding of the function of adiponectin, which may serve to gauge the mitochondrial lipid demand in adipocytes. Adiponectin could therefore act as a powerful systemic signal to drive dietary and tissue lipids toward the adipocyte[5]. However, future studies will need to delineate the detailed mechanistic steps that connect compromised mitochondrial function with the paradoxical increase in adipocyte-derived adiponectin production.

The mitochondrial membrane potential ($\Delta\Psi m$) is a crucial parameter that reflects ETC activity. Considerable loss or depolarization of $\Delta\Psi m$ could lead to low cellular energy[43], as cells with impaired oxidative phosphorylation have low $\Delta\Psi m$[44]. Overexpressing mitoNEET in 3T3-L1 preadipocytes lowers their $\Delta\Psi m$, indicating some degree of energy depletion. Therefore, either overabundance of mitoNEET (compromising mitochondrial function) or a reduction in the amount of mitoNEET (which has the potential for rapid cellular substrate depletion caused by excessive mitochondrial activity) may bring mitochondrial function out of sync with cellular energy requirements, accentuating that the amount of mitoNEET must be harmonized with intracellular energy demands. Alterations in mitoNEET expression further allowed us to manipulate ROS concentrations.

Heightened ROS generation results from severe alterations in oxidative metabolism[31]. Although ROS concentrations intensify with obesity[45], a mitoNEET-induced increase in lipid uptake accompanied by low β-oxidation may alleviate the burden of flux through ROS-producing β-oxidation pathways, thereby protecting adipose tissue from ROS-induced oxidative injury. This paradox of low ROS generation in an oversized, lipid-laden fat pad implies a fully functional ROS-scavenging system. No mitochondrial dysfunction *per se* exists in a mitoNEET-enriched environment; rather, there is an insufficient rate of ETC activity. Interestingly, ROS generation is greater when basal respiration is supported by fatty acids rather than carbohydrate-based substrates[46]. Low β-oxidation rates accompanied by high glycolytic rates caused by mitoNEET overexpression may further sustain low ROS production.

Oxidative stress is also a robust negative correlate of insulin sensitivity[33,36,47]. Despite gaining less body weight during HFD-feeding, mitoNEET knockdown mice have high amounts of ROS-induced protein damage and are less glucose tolerant. ROS generation is prominent when the proton motive force is large[48]; for example, hyperglycemia-induced hyperpolarization elevates ROS production as a result of enhanced cellular respiration[49]. The high $\Delta\Psi m$ after a reduction of mitoNEET expression, accompanied by enhanced oxygen-consumption rates, implicates that ROS may contribute to glucose intolerance. Indeed, other mouse models that are engineered to increase flux through β-oxidation pathways develop severe insulin resistance despite harboring protection from HFD-induced obesity[50]. Our *in vitro* results in this system confirmed that antioxidant treatment of cells with low expression of mitoNEET leads to improvements in cellular insulin signal transduction.

Two key regulators of ETC activity and ROS concentrations are the intracellular redox potential of NAD^+ and NADH, and the proton motive force. A surplus of the reduced equivalents NADH and $FADH_2$, formed through glycolysis and the tricarboxylic acid cycle, are reoxidized through the ETC. Vice versa, a mismatch between β-oxidation and ETC activity disrupts the energy milieu of mitochondria by perturbing redox status[1] to reduce the ratio of NAD^+ to NADH. As an overexpression of mitoNEET lowers the NAD^+:NADH ratio, a buildup of NADH implies that (i) compensatory high glycolytic rates may generate surplus NADH from the decline in β-oxidation, (ii) ETC activity is insufficient to reoxidize NADH, (iii) mitoNEET may affect NAD and NADH flux through various catabolic pathways or (iv) mitoNEET may alter NAD shuttle systems, salvage or degradation such that mitochondrial performance is further perturbed by rising NADH concentrations[1].

Low mitochondrial iron content can decrease the activity of iron-containing ETC complexes and enzymes to diminish respiratory activity[26]. An excess of mitoNEET causes reduced concentrations of mitochondrial iron, and vice versa, a reduction in the amount of mitoNEET causes an increase in iron concentrations and ETC activity. This pinpoints iron transport as one of the crucial aspects of mitoNEET function. Indeed, researchers from a recent study showed that iron overload (in the context of hereditary hemochromatosis) is associated with a shift from glucose to fatty acid oxidation and an increased risk of developing diabetes[28]. These observations are fully consistent with the findings reported here in which a downregulation of mitoNEET led to similar phenotypic manifestations.

In summary, we identify the mitochondrial protein mitoNEET as a valuable tool in energy homeostasis and lipid metabolism. We used mitoNEET as a genetic tool to manipulate ETC activity by taking advantage of its ability to exert control over mitochondrial iron availability. We show that within the adipocyte, mitoNEET compromises mitochondrial efficacy, triggers a massive nutrient influx into the cell, enhances adiponectin production and increases β-3 adrenergic sensitivity. The increased lipid influx, combined with reduced oxidative capacity, initiates massive adipose tissue expansion; despite the resulting obesity, insulin sensitivity is preserved. Several of these effects are probably dependent on a mitoNEET-mediated induction of adiponectin. Such mitoNEET-driven alterations in mitochondrial function therefore represent pivotal mechanisms that link obesity-related insulin resistance with mitochondrial perturbations and, further, open the door to effective manipulation of mitochondrial activity in additional cell types. Although a higher mitochondrial concentration of mitoNEET protein in adipocytes promotes further obesity, it also triggers enhanced adiponectin release and, thus, improved insulin sensitivity.

The association of increased obesity with improvements in insulin sensitivity is counterintuitive. However, the obesity-associated toning down of mitochondrial activity could serve as an adaptive process in an attempt by cells to counter the effects of excess lipid intake. We therefore suggest that a moderate reduction in mitochondrial oxidative phosphorylation specifically in the sWAT fat pad paradoxically favors beneficial metabolic outcomes. MitoNEET drives an adipocyte to preferentially store lipids, concomitant with a decreased propensity to oxidize them. In particular, our bioenergetic profiling reveals that mitoNEET-overexpressing mitochondria have low oxygen-consumption rates in response to various substrates. In contrast, an environment deficient in mitoNEET enhances lipid- and carbohydrate-based respiration. Taken together, we propose an inverse correlation between mitoNEET and oxidative capacity, a phenomenon that, when operational in the subcutaneous fat pad, drives an effective improvement in whole-body metabolism. To better understand the regulation of this process under normal physiological conditions, our future studies will focus on the regulation of endogenous mitoNEET and its detailed molecular mechanism of action. Furthermore, a better understanding of how altered energetic states of mitochondria affect adiponectin production, assembly and release deserves more attention in light of the potent metabolic improvements triggered by even moderate changes in cellular and plasma adiponectin concentrations.

METHODS

Methods and any associated references are available in the online version of the paper.

Accession codes. The microarray data have been uploaded to the Gene Expression Omnibus database under accession code GSE39251.

Note: Supplementary information is available in the online version of the paper.

ACKNOWLEDGMENTS

We thank P.D. Neufer, G. Schatz and C.B. Newgard for helpful comments and suggestions. We also thank J. Song and J. Xia for technical assistance, in addition to the rest of the Scherer laboratory, R. Unger and D. Clegg for helpful discussions. We also thank P. Blanchard and Y. Deshaies for kindly providing LPL activity measurements, R. Hammer and the University of Texas Southwestern (UTSW) Transgenic Core Facility for the generation of mouse models, as well as the UTSW Metabolic Core Facility for help in the phenotypic characterization of the mice and G. Milne from Vanderbilt University Medical Center for the F2-isoprostane analysis. The authors were supported by US National Institutes of Health grants R01-DK55758, RC1-DK086629 and P01-DK088761 (P.E.S.), K99-DK094973 and an American Heart Association Beginning Grant in Aid 12BGIA8910006 (W.L.H.), R01-DK081842 (D.A.M.), T32-DK091317 (J.A.S.) and Department of Defense Fellowship USAMRMC-BC085909 (J.P.). C.M.K. was supported by a fellowship from the Juvenile Diabetes Foundation (JDRF 3-2008-130).

AUTHOR CONTRIBUTIONS

C.M.K. conducted all experiments and wrote the manuscript, except the portions indicated below. W.L.H. helped with the ^{3}H-triolein uptake and β-oxidation experiments and performed their analyses. K.S. generated TRE-mitoNEET mice. J.P. helped plan, perform injections and scan fat pads in control AAV and AAV-mitoNEET experiments. S.B.S. generated the AAV-mitoNEET construct. Y.L. performed the $DiOC_6$ $\Delta\Psi m$ experiment using mitoNEET-transfected 3T3-L1 preadipocytes. G.R.A. and C.L. coordinated the generation of shRNA-MitoN knockdown mice. J.A.S. and D.A.M. measured heme iron and provided high-iron-diet–fed and *Hfe*$^{-/-}$ liver tissues. P.E.S. was involved in the experimental design, experiments, data analysis and data interpretation, in addition to writing the manuscript.

COMPETING FINANCIAL INTERESTS

The authors declare no competing financial interests.

Published online at http://www.nature.com/doifinder/10.1038/nm.2899.
Reprints and permissions information is available online at http://www.nature.com/reprints/index.html.

1. Muoio, D.M. & Newgard, C.B. Obesity-related derangements in metabolic regulation. *Annu. Rev. Biochem.* **75**, 367–401 (2006).
2. Lowell, B.B. & Shulman, G.I. Mitochondrial dysfunction and type 2 diabetes. *Science* **307**, 384–387 (2005).
3. Mehta, J.L., Rasouli, N., Sinha, A.K. & Molavi, B. Oxidative stress in diabetes: a mechanistic overview of its effects on atherogenesis and myocardial dysfunction. *Int. J. Biochem. Cell Biol.* **38**, 794–803 (2006).
4. Morino, K., Petersen, K.F. & Shulman, G.I. Molecular mechanisms of insulin resistance in humans and their potential links with mitochondrial dysfunction. *Diabetes* **55** (suppl. 2), S9–S15 (2006).
5. Kim, J.Y. *et al.* Obesity-associated improvements in metabolic profile through expansion of adipose tissue. *J. Clin. Invest.* **117**, 2621–2637 (2007).
6. Scherer, P.E., Williams, S., Fogliano, M., Baldini, G. & Lodish, H.F. A novel serum protein similar to C1q, produced exclusively in adipocytes. *J. Biol. Chem.* **270**, 26746–26749 (1995).
7. Holland, W.L. *et al.* Receptor-mediated activation of ceramidase activity initiates the pleiotropic actions of adiponectin. *Nat. Med.* **17**, 55–63 (2011).
8. Kelley, D.E., He, J., Menshikova, E.V. & Ritov, V.B. Dysfunction of mitochondria in human skeletal muscle in type 2 diabetes. *Diabetes* **51**, 2944–2950 (2002).
9. Ritov, V.B. *et al.* Deficiency of subsarcolemmal mitochondria in obesity and type 2 diabetes. *Diabetes* **54**, 8–14 (2005).
10. Simoneau, J.A., Veerkamp, J.H., Turcotte, L.P. & Kelley, D.E. Markers of capacity to utilize fatty acids in human skeletal muscle: relation to insulin resistance and obesity and effects of weight loss. *FASEB J.* **13**, 2051–2060 (1999).
11. Colca, J.R. *et al.* Identification of a novel mitochondrial protein ("mitoNEET") cross-linked specifically by a thiazolidinedione photoprobe. *Am. J. Physiol. Endocrinol. Metab.* **286**, E252–E260 (2004).
12. Paddock, M.L. *et al.* MitoNEET is a uniquely folded 2Fe 2S outer mitochondrial membrane protein stabilized by pioglitazone. *Proc. Natl. Acad. Sci. USA* **104**, 14342–14347 (2007).
13. Wiley, S.E., Murphy, A.N., Ross, S.A., van der Geer, P. & Dixon, J.E. MitoNEET is an iron-containing outer mitochondrial membrane protein that regulates oxidative capacity. *Proc. Natl. Acad. Sci. USA* **104**, 5318–5323 (2007).
14. Wiley, S.E. *et al.* The outer mitochondrial membrane protein mitoNEET contains a novel redox-active 2Fe-2S cluster. *J. Biol. Chem.* **282**, 23745–23749 (2007).
15. Lin, J., Zhou, T., Ye, K. & Wang, J. Crystal structure of human mitoNEET reveals distinct groups of iron sulfur proteins. *Proc. Natl. Acad. Sci. USA* **104**, 14640–14645 (2007).
16. Graves, R.A., Tontonoz, P., Platt, K.A., Ross, S.R. & Spiegelman, B.M. Identification of a fat cell enhancer: analysis of requirements for adipose tissue-specific gene expression. *J. Cell. Biochem.* **49**, 219–224 (1992).
17. Chavez, J.A. & Summers, S.A. A ceramide-centric view of insulin resistance. *Cell Metab.* **15**, 585–594 (2012).
18. Jornayvaz, F.R. & Shulman, G.I. Diacylglycerol activation of protein kinase cepsilon and hepatic insulin resistance. *Cell Metab.* **15**, 574–584 (2012).
19. Milne, G.L., Sanchez, S.C., Musiek, E.S. & Morrow, J.D. Quantification of F2-isoprostanes as a biomarker of oxidative stress. *Nat. Protoc.* **2**, 221–226 (2007).
20. Langin, D. Adipose tissue lipolysis as a metabolic pathway to define pharmacological strategies against obesity and the metabolic syndrome. *Pharmacol. Res.* **53**, 482–491 (2006).
21. Asterholm, I.W. & Scherer, P.E. Enhanced metabolic flexibility associated with elevated adiponectin levels. *Am. J. Pathol.* **176**, 1364–1376 (2010).
22. Franckhauser, S. *et al.* Increased fatty acid re-esterification by PEPCK overexpression in adipose tissue leads to obesity without insulin resistance. *Diabetes* **51**, 624–630 (2002).
23. Hanson, R.W. & Reshef, L. Glyceroneogenesis revisited. *Biochimie* **85**, 1199–1205 (2003).
24. Sun, K., Kusminski, C.M. & Scherer, P.E. Adipose tissue remodeling and obesity. *J. Clin. Invest.* **121**, 2094–2101 (2011).
25. Zuris, J.A. *et al.* Facile transfer of [2Fe-2S] clusters from the diabetes drug target mitoNEET to an apo-acceptor protein. *Proc. Natl. Acad. Sci. USA* **108**, 13047–13052 (2011).
26. Macdonald, V.W., Charache, S. & Hathaway, P.J. Iron deficiency anemia: mitochondrial α-glycerophosphate dehydrogenase in guinea pig skeletal muscle. *J. Lab. Clin. Med.* **105**, 11–18 (1985).
27. Crooks, D.R., Ghosh, M.C., Haller, R.G., Tong, W.H. & Rouault, T.A. Posttranslational stability of the heme biosynthetic enzyme ferrochelatase is dependent on iron availability and intact iron-sulfur cluster assembly machinery. *Blood* **115**, 860–869 (2010).
28. Huang, J. *et al.* Iron overload and diabetes risk: a shift from glucose to fatty acid oxidation and increased hepatic glucose production in a mouse model of hereditary hemochromatosis. *Diabetes* **60**, 80–87 (2011).
29. Mitchell, P. Keilin's respiratory chain concept and its chemiosmotic consequences. *Science* **206**, 1148–1159 (1979).
30. Rogers, G.W. *et al.* High throughput microplate respiratory measurements using minimal quantities of isolated mitochondria. *PLoS ONE* **6**, e21746 (2011).
31. Rigoulet, M., Yoboue, E.D. & Devin, A. Mitochondrial ROS generation and its regulation: mechanisms involved in H_2O_2 signaling. *Antioxid. Redox Signal.* **14**, 459–468 (2011).
32. Wu, M. *et al.* Multiparameter metabolic analysis reveals a close link between attenuated mitochondrial bioenergetic function and enhanced glycolysis dependency in human tumor cells. *Am. J. Physiol. Cell Physiol.* **292**, C125–C136 (2007).

33. Houstis, N., Rosen, E.D. & Lander, E.S. Reactive oxygen species have a causal role in multiple forms of insulin resistance. *Nature* **440**, 944–948 (2006).
34. Tarnopolsky, M.A. *et al.* Influence of endurance exercise training and sex on intramyocellular lipid and mitochondrial ultrastructure, substrate use, and mitochondrial enzyme activity. *Am. J. Physiol. Regul. Integr. Comp. Physiol.* **292**, R1271–R1278 (2007).
35. Lin, J., Puigserver, P., Donovan, J., Tarr, P. & Spiegelman, B.M. Peroxisome proliferator-activated receptor γ coactivator 1β (PGC-1β), a novel PGC-1–related transcription coactivator associated with host cell factor. *J. Biol. Chem.* **277**, 1645–1648 (2002).
36. Bonnard, C. *et al.* Mitochondrial dysfunction results from oxidative stress in the skeletal muscle of diet-induced insulin-resistant mice. *J. Clin. Invest.* **118**, 789–800 (2008).
37. Curtis, J.M. *et al.* Downregulation of adipose glutathione S-transferase A4 leads to increased protein carbonylation, oxidative stress, and mitochondrial dysfunction. *Diabetes* **59**, 1132–1142 (2010).
38. Karelis, A.D. *et al.* The metabolically healthy but obese individual presents a favorable inflammation profile. *J. Clin. Endocrinol. Metab.* **90**, 4145–4150 (2005).
39. McGarry, J.D. Banting lecture 2001: dysregulation of fatty acid metabolism in the etiology of type 2 diabetes. *Diabetes* **51**, 7–18 (2002).
40. Koh, E.H. *et al.* Essential role of mitochondrial function in adiponectin synthesis in adipocytes. *Diabetes* **56**, 2973–2981 (2007).
41. Frizzell, N. *et al.* Succination of thiol groups in adipose tissue proteins in diabetes: succination inhibits polymerization and secretion of adiponectin. *J. Biol. Chem.* **284**, 25772–25781 (2009).
42. Iwabu, M. *et al.* Adiponectin and AdipoR1 regulate PGC-1α and mitochondria by Ca^{2+} and AMPK/SIRT1. *Nature* **464**, 1313–1319 (2010).
43. Sherratt, H.S. Mitochondria: structure and function. *Rev. Neurol. (Paris)* **147**, 417–430 (1991).
44. Dey, R. & Moraes, C.T. Lack of oxidative phosphorylation and low mitochondrial membrane potential decrease susceptibility to apoptosis and do not modulate the protective effect of Bcl-x(L) in osteosarcoma cells. *J. Biol. Chem.* **275**, 7087–7094 (2000).
45. Furukawa, S. *et al.* Increased oxidative stress in obesity and its impact on metabolic syndrome. *J. Clin. Invest.* **114**, 1752–1761 (2004).
46. Anderson, E.J., Yamazaki, H. & Neufer, P.D. Induction of endogenous uncoupling protein 3 suppresses mitochondrial oxidant emission during fatty acid–supported respiration. *J. Biol. Chem.* **282**, 31257–31266 (2007).
47. Anderson, E.J. *et al.* Mitochondrial H_2O_2 emission and cellular redox state link excess fat intake to insulin resistance in both rodents and humans. *J. Clin. Invest.* **119**, 573–581 (2009).
48. Korshunov, S.S., Skulachev, V.P. & Starkov, A.A. High protonic potential actuates a mechanism of production of reactive oxygen species in mitochondria. *FEBS Lett.* **416**, 15–18 (1997).
49. Yu, T., Robotham, J.L. & Yoon, Y. Increased production of reactive oxygen species in hyperglycemic conditions requires dynamic change of mitochondrial morphology. *Proc. Natl. Acad. Sci. USA* **103**, 2653–2658 (2006).
50. Finck, B.N. *et al.* A potential link between muscle peroxisome proliferator- activated receptor-α signaling and obesity-related diabetes. *Cell Metab.* **1**, 133–144 (2005).

ONLINE METHODS

Mice. All animal experimental protocols were approved by the Institutional Animal Care and Use Committee of University of Texas Southwestern Medical Center at Dallas. Adipose-specific mitoNEET transgenic mice were generated by subcloning the mitoNEET gene into a plasmid containing the 5.4-kb aP2 promoter and a conventional 3′ untranslated region[5]. After linearization, the construct was injected into FVB-derived blastocysts. Transgene-positive offspring were genotyped using PCR with the primer set 5′-GGACCTCTGATCATCAAGA-3′ and 5′-GGAGACAATGGTTGTCAAC-3′. All overexpression experiments were performed in a pure FVB background. Adiponectin-null mice were previously described[51]. Generation of doxycycline-inducible shRNA-mitoN knockdown and mitoNEET overexpression mouse models are detailed in the **Supplementary Methods**. All experiments were conducted using littermate-controlled male or female mice. All HFD experiments were initiated at 6–12 weeks of age. Mice were fed a standard chow diet (number 5058, LabDiet), a Dox-chow diet (600 mg kg^{-1} Dox; Bio-Serv), a 60% HFD (D12492, Research Diets Inc.) or a Dox-HFD (600 mg kg^{-1} Dox; Bio-Serv).

Systemic tests. For OGTTs, mice were fasted for 3 h before administration of glucose (2.5 g per kg body weight by gastric gavage). Glucose concentrations were measured using an oxidase-peroxidase assay (Sigma-Aldrich). For triglyceride clearance, mice were fasted (16 h), then gavaged with 15 µl per g body weight of 20% intralipid (Fresenius Kabi Clyton, L.P.). Blood was collected at timed intervals and then assayed for triglyceride (Infinity; Thermo Fisher Scientific) and FFA concentrations (NEFA-HR(2); Wako Pure Chemical Industries). For β-3 adrenergic receptor agonist tests, blood samples were obtained before and 5, 15, 60 and 120 min after intraperitoneal injection of 1 mg kg^{-1} CL316,243 (Sigma-Aldrich). Insulin and adiponectin concentrations were measured using commercial ELISA kits (Millipore Linco Research). Glycerol and glucose concentrations were determined using a free glycerol reagent and an oxidase-peroxidase assay, respectively (Sigma-Aldrich).

Hyperinsulinemic-euglycemic clamps. Hyperinsulinemic-euglycemic clamps were performed on conscious, unrestrained 10-week-old male FVB *ob*/*ob* and MitoN-Tg *ob*/*ob* mice, as previously described[7,52].

Quantitative RT-PCR and microarray. Tissues were excised from mice and snap frozen. Total RNA was isolated after tissue homogenization in TRIzol (Invitrogen) and then isolated using an RNeasy RNA extraction kit (Qiagen). Complementary DNA was prepared by reverse transcribing 1 µg of RNA with SuperScript III reverse transcriptase and oligo$(dT)_{20}$ (Invitrogen). **Supplementary Table 2** lists the primer sets used for quantitative RT-PCR. Results were calculated using the threshold cycle method[53], with β-actin used for normalization. For the microarray, total complementary DNA was synthesized from sWAT and then spotted onto a mouse Illumina BeadArray platform (Illumina, Inc.). Fold changes and statistical significance were calculated based on three independent replicates. Gene lists and cluster analyses of the datasets were performed using Ingenuity software (Ingenuity Systems Inc.).

Immunoblotting. Frozen tissue was homogenized in TNET buffer (50 mM Tris-HCl, pH 7.6, 150 mM NaCl, 5 mM EDTA, phosphatase inhibitors (Sigma-Aldrich) and protease inhibitors (Roche)) and then centrifuged to remove any adipose layer present. After the addition of Triton X-100 (final concentration of 1%), protein concentrations were determined using a bicinchoninic acid assay (BCA) kit (Pierce). Proteins were resolved on 4–12% Bis-Tris gels (Invitrogen) or 10–20% Tricine gels (Invitrogen) and then transferred to polyvinylidene difluoride membranes (Millipore) and nitrocellulose membranes (Protran, Whatman GmbH), respectively. A rabbit polyclonal antibody was raised against mouse mitoNEET with purified protein of a C-terminal fusion of full-length murine mitoNEET to glutathione S-transferase (1:1,000). Adiponectin-specific antibodies (1:1,000) were used, as previously described[54]. pAkt (Ser473, 4060) and total Akt (2920) (Cell Signaling Technology, Inc.) were used (1:1,000) for insulin signaling studies. Primary antibodies were detected using secondary IgG labeled with infrared dyes emitting at 700 nm (926-32220) or 800 nm (926-32211) (both at 1:5,000 dilutions) (Li-Cor Bioscience) and then visualized on a Li-Cor Odyssey infrared scanner (Li-Cor Bioscience). The scanned data were analyzed using Odyssey Version 2.1 software (Li-Cor Bioscience). The complex distribution of adiponectin was determined as previously described[5]. Tissue LPL activity was determined as previously detailed[55]. NAD^+ and NADH concentrations were assessed according to the manufacturer's instructions (BioVision Inc.). Iron content was measured using commercial kits (BioAssay Systems). Hepatic ceramide and hepatic diacylglycerol concentrations were determined as previously detailed[7].

Histology and immunohistochemistry. Fat pads or liver tissues were excised and fixed in 10% PBS-buffered formalin for 24 h. After paraffin embedding and sectioning (5 µm), tissues were stained with H&E or a Masson's trichrome stain. For immunohistochemistry, paraffin-embedded sections were stained using monoclonal antibodies to Mac2 (1:1,000, CL8942AP, CEDARLANE Laboratories USA Inc.).

Preparation of MEFs and isolation of mitochondria. MEFs were derived from WT or shRNA-mitoN embryonic day (E) 13.5 embryos with a C57BL/6J background. MEFs were cultured in DMEM containing glutamine, nonessential amino acids, penicillin and streptomycin, 20 mM 4-(2-hydroxyethyl)-1-piperazineethanesulfonic acid (HEPES) and 10% FBS at 37 °C under 5% CO_2. For insulin signaling studies, WT and shRNA-mitoN MEFs were cultured in Dox-containing DMEM (1 µg ml^{-1}), then treated with either palmitate (400 µM; Sigma-Aldrich) or MnTBAP (1 mg ml^{-1}; Cayman Chemical Company) for 4 h. Cells were then acutely treated with insulin (16 nM; Sigma-Aldrich) for 10 min before cell harvesting and protein extraction for western blot analysis. To isolate mitochondria, fresh tissues were homogenized using a drill-operated Teflon pestle in ice-cold MSHE buffer (70 mM sucrose, 210 mM mannitol, 5 mM HEPES and 1 mM EDTA) containing either 4% fatty-acid–free BSA (for adipose tissue) or 0.5% fatty-acid–free BSA (for liver). After low centrifugation (800 *g* for 10 min) and then high centrifugation (8,000 *g* for 10 min), the mitochondrial pellet was resuspended in the corresponding MSHE buffer, and protein concentrations were determined using a BCA kit (Pierce).

Mitochondrial experiments. OCR and ECAR values were determined using the XF24 Extracellular Flux Analyzer (Seahorse Bioscience) following the manufacturer's protocols. For β-oxidation, WT MEFs and shRNA-mitoN MEFs (60,000 per well; 1 µg ml^{-1} Dox) were seeded overnight in a XF24 cell culture microplate at 37 °C under 5% CO_2 (Seahorse Bioscience). After a 1-h equilibration with 1X KHB buffer (111 mM NaCl, 4.7 mM KCl, 2 mM $MgSO_4$ and 1.2 mM Na_2HPO_4) supplemented with 0.5 mM carnitine and 2.5 mM glucose, cells were subjected to treatment of a palmitate-BSA conjugate (200 µM; C:16:0), followed by treatment with etomoxir (100 µM). OCR measurements were recorded at set interval time points. For electron-flow measurements, isolated mitochondria were pelleted in an XF24 cell-culture microplate by centrifugation (2,000*g* for 20 min at 4 °C) in 1× MAS buffer (70 mM sucrose, 220 mM mannitol, 10 mM KH_2PO_4, 5 mM $MgCl_2$, 2 mM HEPES and 1 mM EDTA in 0.2% FA-free BSA) supplemented with 10 mM pyruvate, 10 mM malate and 4 µM FCCP. OCR and ECAR measurements were obtained after sequential additions of rotenone (2 µM final concentration), succinate (10 mM), antimycin A (4 µM) and ascorbate (10 mM) (the latter containing 1 mM TMPD). For ECAR glycolytic flux experiments using whole-tissue slices, oligomycin (2 µM), FCCP (4 µM), 2-deoxyglucose (2-DG) (100 mM) and antimycin A (10 µM) were added to tissues in an XF24 islet-capture Microplate (Seahorse Bioscience). All compounds and materials above were obtained from Sigma-Aldrich. For mitochondrial oxidative stress, the protein carbonylation assay was performed as previously described[37]. For lipid peroxidation, amounts of bound 8-isoPGF2α were determined as previously detailed[19]. The mitochondrial membrane potential ($\Delta\Psi m$) experiments are detailed in the **Supplementary Methods**.

^{3}H-triolein uptake and β-oxidation. For measurements of endogenous triolein clearance rates, tissue-specific lipid uptake and β-oxidation rates in transgenic tissues, methodologies were adapted from previously detailed studies[56,57]. Briefly, ^{3}H-triolein was tail-vein injected (2 µCi per mouse in 100 µl of 5% intralipid) into mice after a 16 h fast. Briefly, blood samples (0.15 ml) were then collected at 1, 2, 5, 10 and 15 min after injection. At 20 min following injection, mice were euthanized, blood samples were taken and tissues were

doi:10.1038/nm.2899

quickly excised, weighed and frozen at −80 °C until processing. Lipids were then extracted using a chloroform-to-methanol based extraction method[58]. The radioactivity content of tissues, including blood samples, was quantified as described previously[57].

Statistics. All results are provided as means ± s.e.m. All statistical analyses were performed using GraphPad Prism. Differences between the two groups over time (indicated in the relevant figure legends) were determined by a two-way analysis of variance for repeated measures. For comparisons between two independent groups, a Student's *t* test was used. Significance was accepted at $P < 0.05$.

51. Nawrocki, A.R. *et al.* Mice lacking adiponectin show decreased hepatic insulin sensitivity and reduced responsiveness to peroxisome proliferator-activated receptor γ agonists. *J. Biol. Chem.* **281**, 2654–2660 (2006).
52. Berglund, E.D. *et al.* Direct leptin action on POMC neurons regulates glucose homeostasis and hepatic insulin sensitivity in mice. *J. Clin. Invest.* **122**, 1000–1009 (2012).
53. Livak, K.J. & Schmittgen, T.D. Analysis of relative gene expression data using real-time quantitative PCR and the $2^{-\Delta\Delta C(T)}$ method. *Methods* **25**, 402–408 (2001).
54. Scherer, P.E., Williams, S., Fogliano, M., Baldini, G. & Lodish, H.F. A novel serum protein similar to C1q, produced exclusively in adipocytes. *J. Biol. Chem.* **270**, 26746–26749 (1995).
55. Combs, T.P. *et al.* A transgenic mouse with a deletion in the collagenous domain of adiponectin displays elevated circulating adiponectin and improved insulin sensitivity. *Endocrinology* **145**, 367–383 (2004).
56. Laplante, M. *et al.* Tissue-specific postprandial clearance is the major determinant of PPARγ-induced triglyceride lowering in the rat. *Am. J. Physiol. Regul. Integr. Comp. Physiol.* **296**, R57–R66 (2009).
57. Hultin, M., Carneheim, C., Rosenqvist, K. & Olivecrona, T. Intravenous lipid emulsions: removal mechanisms as compared to chylomicrons. *J. Lipid Res.* **36**, 2174–2184 (1995).
58. Bligh, E.G. & Dyer, W.J. A rapid method of total lipid extraction and purification. *Can. J. Biochem. Physiol.* **37**, 911–917 (1959).

MitoNEET-driven alterations in adipocyte mitochondrial activity reveal a crucial adaptive process that preserves insulin sensitivity in obesity

Christine M. Kusminski, William L. Holland, Kai Sun, Jiyoung Park, Stephen Spurgin, Ying Lin, G Roger Askew, Judith A. Simcox, Don A. McClain, Cai Li and Philipp E. Scherer

Supplementary Information

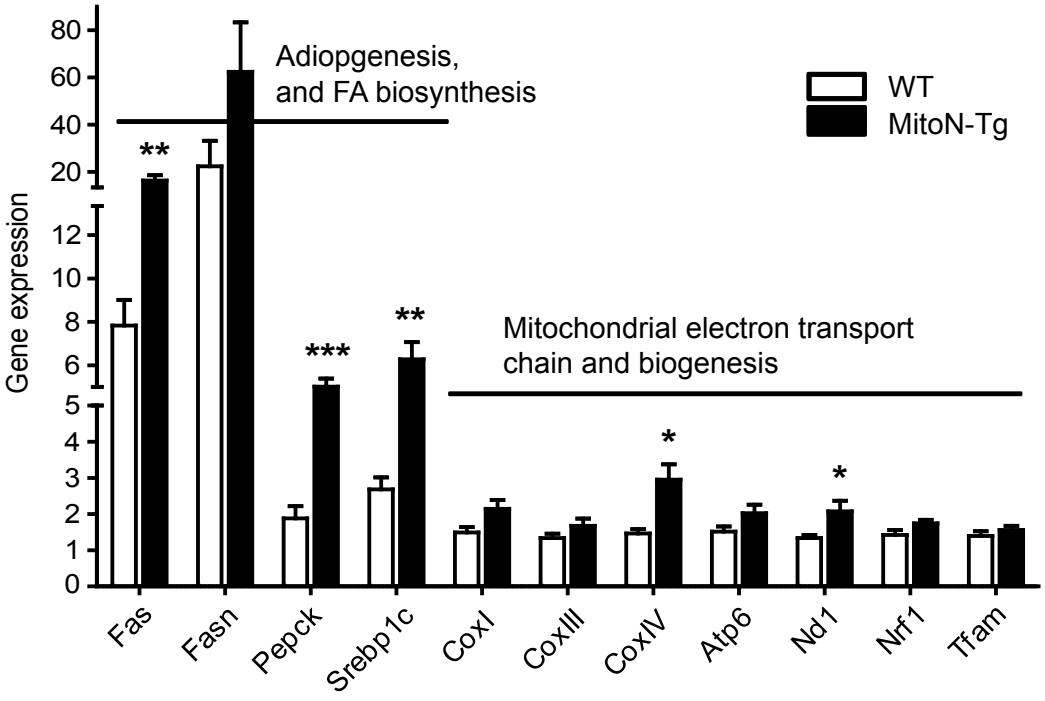

Supplemental Figure 1. Adipogenesis, FA-biosynthesis and mitochondrial pathways are upregulated in MitoN-Tg sWAT. RT-PCR confirmation of key genes obtained from microarray analyses of WT versus MitoN-Tg sWAT (*n* = 9 per group).

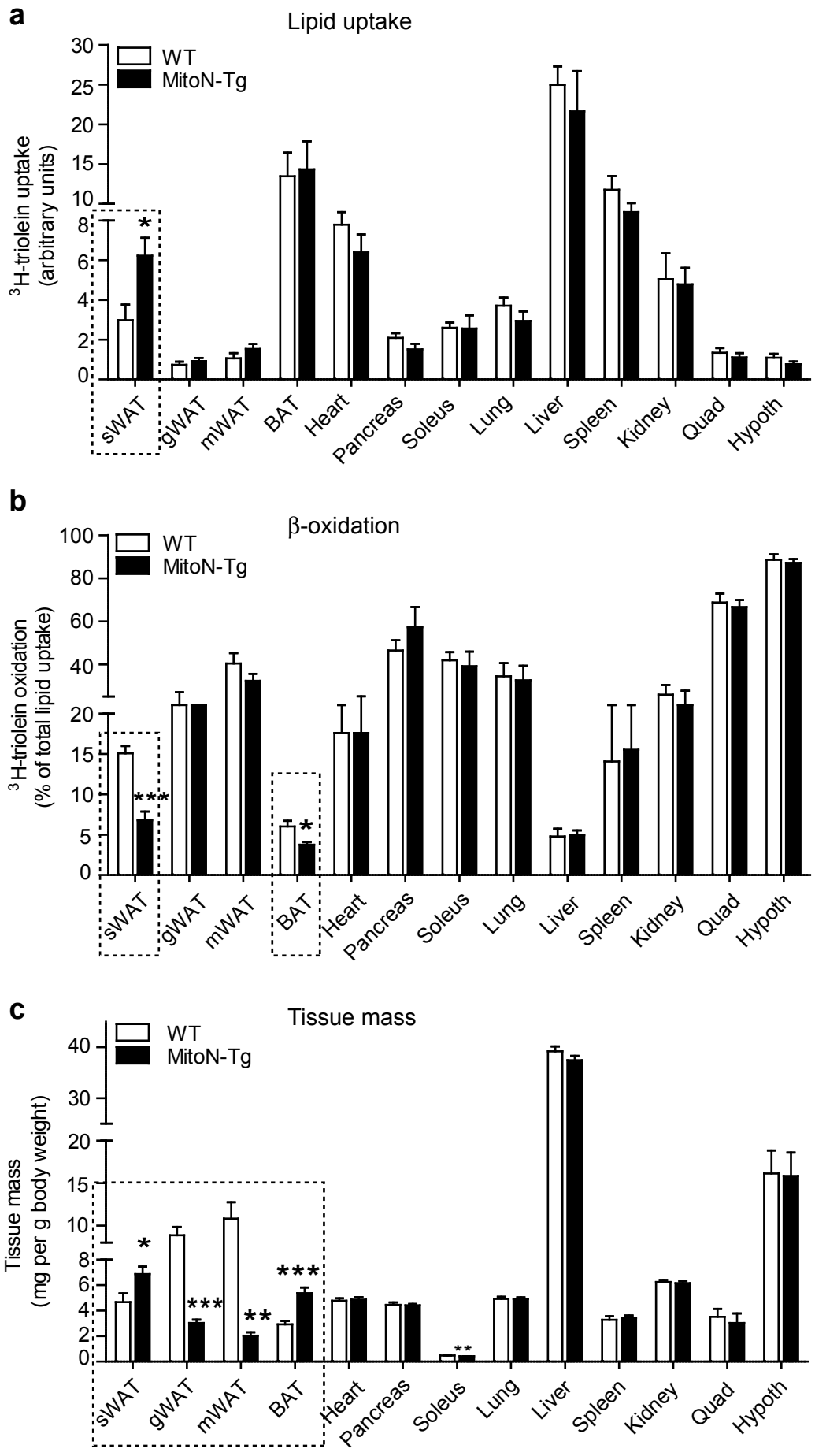

Supplemental Figure 2. MitoNEET enhances lipid-uptake and declines the rate of β-oxidation specifically in sWAT. (a) ^{3}H-triolein lipid-uptake, (b) β-oxidation and (c) tissue-mass in WT versus MitoN-Tg tissues (2 μCi/mouse in 100 ul of 5% intralipid; single tail-vein injection) (*n* = 6 per group).

Nature Medicine doi:10.1038/nm.2899

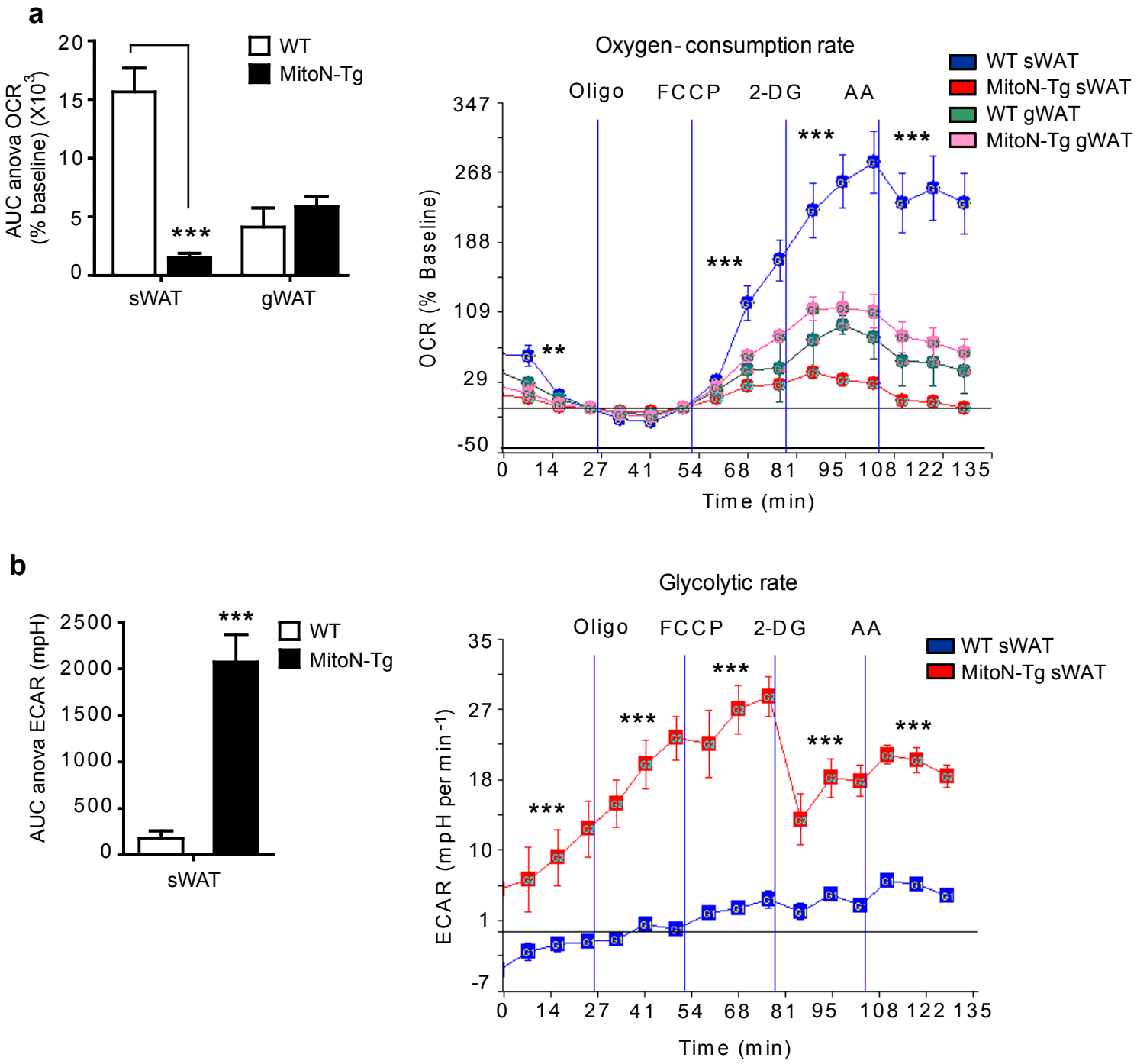

Supplemental Figure 3. Adipose-specific overexpression of mitoNEET enhances glycolysis. Oxygen consumption rates (OCRs) (top-panel) in WT and MitoN-Tg whole sWAT and gWAT tissue-slices (~20 mg), in addition to extracellular acidification rates (ECARs) (bottom panel) (as a measure of glycolytic rate) in WT and MitoN-Tg sWAT tissue-slices; in response to sequential additions of oligomycin (an ATP synthase inhibitor), FCCP (a chemical uncoupler), 2-Deoxy-D-glucose (2-DG) (an inhibitor of glycolysis) and antimycin-A (complex III inhibitor) (n = 4 per group). $^{**}P < 0.01$; $^{***}P < 0.001$.

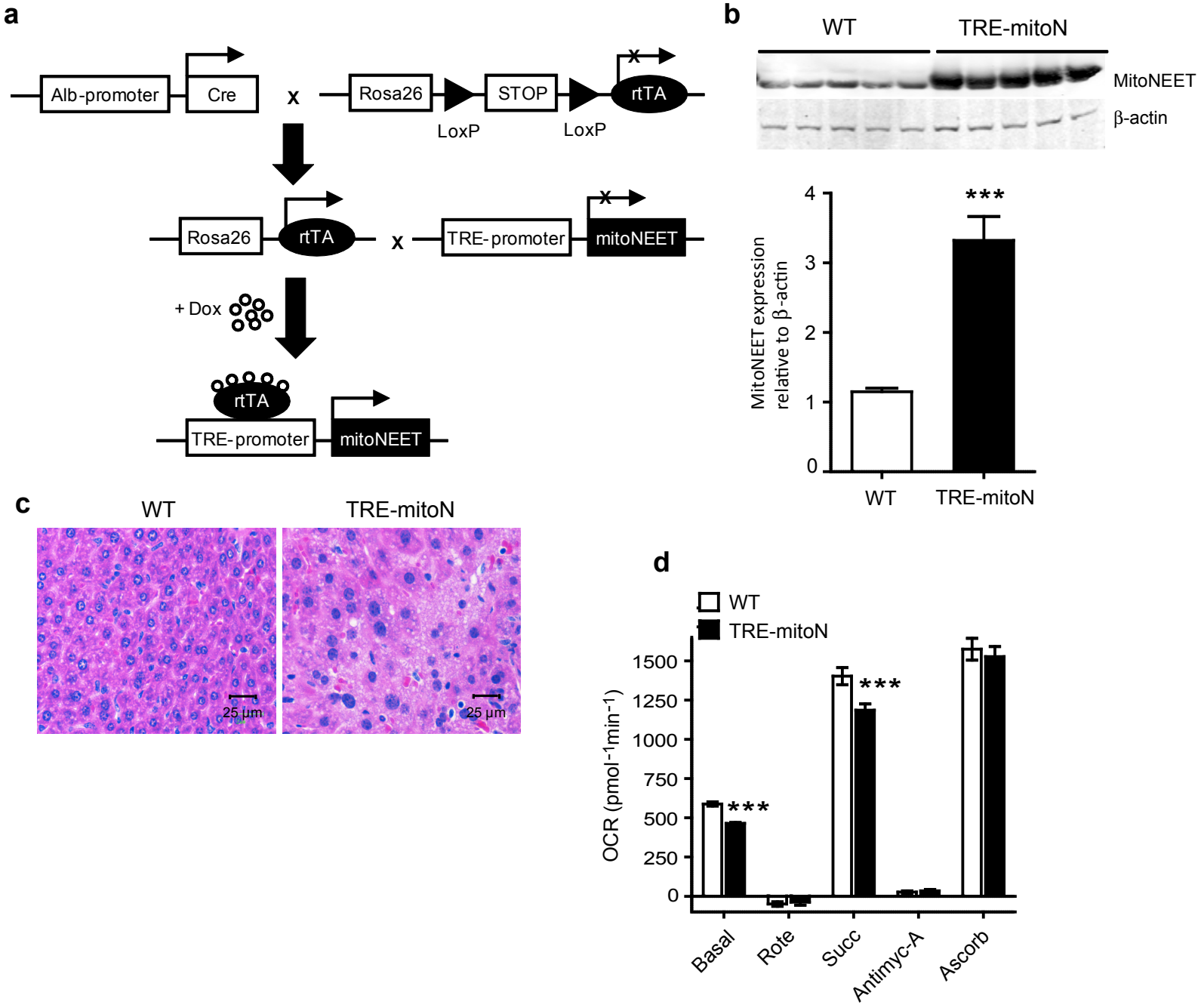

Supplemental Figure 4. Generation of an inducible liver-specific overexpression of mitoNEET. (a) Strategy of Dox-inducible overexpression of mitoNEET specifically in the liver. Liver-specific albumin (Alb)-Cre mice were crossed with the Rosa26-loxP-STOP-loxP-rtTA mice to achieve liver-specific expression of rtTA. These mice were then bred with TRE-mitoN transgenic mice. Following exposure to Dox, the resulting triple transgenic mice express mitoNEET only in the liver. (b) Representative Western blots and the average Dox-induced overexpression of mitoNEET protein in liver tissues from WT and TRE-MitoN mice following Dox-HFD-feeding (600 mg/kg Dox-HFD for 3-weeks) (*n* = 5 per group). (c) Representative H&E stain of WT and TRE-MitoN livers following Dox-HFD feeding. (d) OCRs in mitochondria isolated from WT livers and TRE-mitoN livers (*n* = 5 per group).

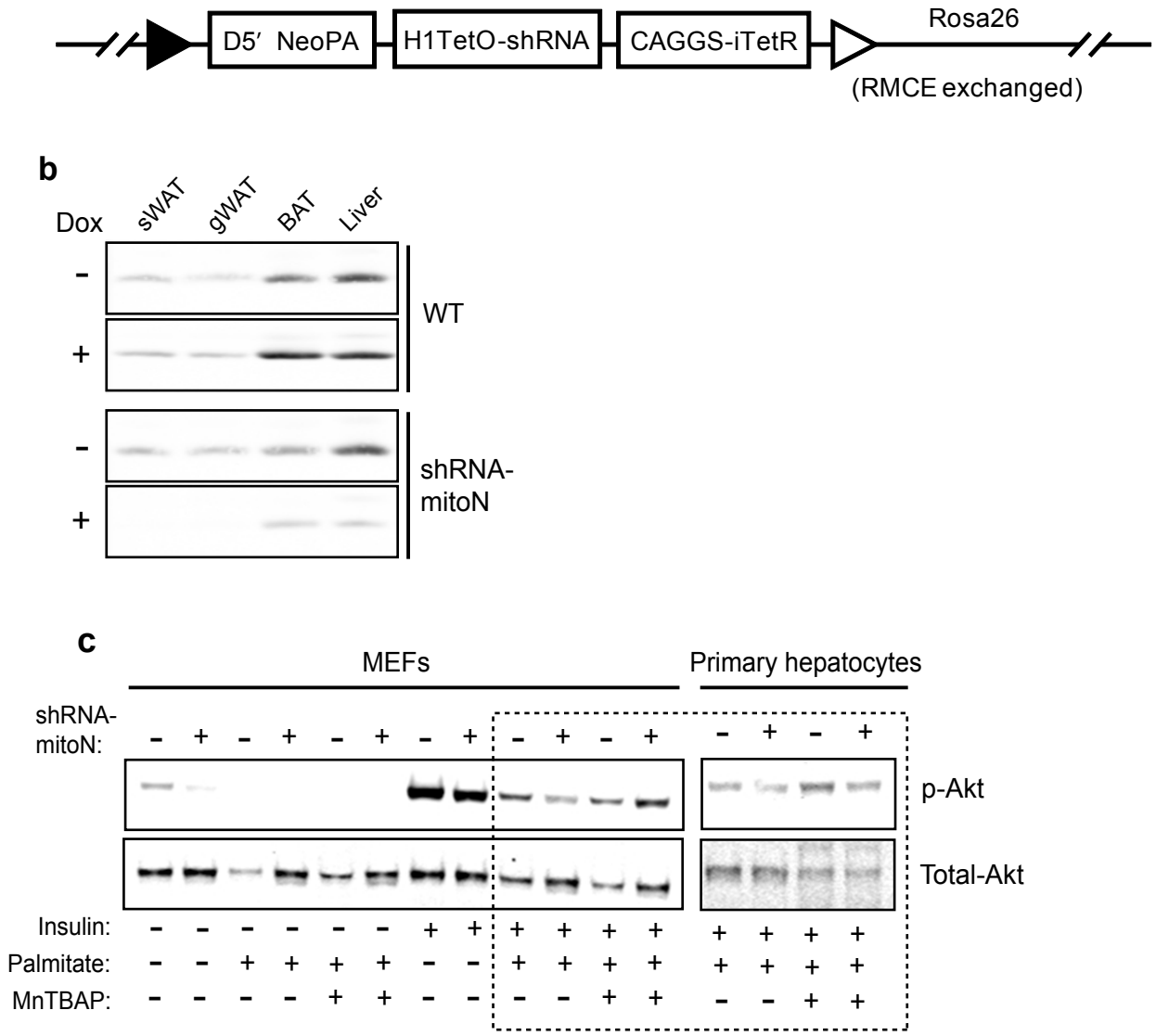

Supplemental Figure 5. Generation of an inducible constitutive knockdown of mitoNEET. (a) Schematic of the Dox-inducible knockdown system of mitoNEET, with the shRNA construct being targeted to the Rosa26 locus. (b) Representative Western blots demonstrating the Dox-induced knockdown of mitoNEET protein in sWAT, gWAT, BAT and liver tissues from WT and shRNA-MitoN mice following Dox-chow-feeding (600 mg/kg Dox-chow for 10 d) (+Dox) or standard chow-feeding (-Dox) (*n* = 4 per group). (c) Representative Western blots showing insulin signaling (phospho-Akt (Ser473) (p-Akt) and total-Akt) in Dox-treated (1 mg/ml) WT and shRNA-mitoN MEFs (left panel), in addition to primary hepatocytes (right panel) derived from WT mice and shRNA-mitoN mice. Expression levels were examined in response to treatments with, or without insulin, palmitate and the anti-oxidant, MnTBAP (*n* = 4 per group).

Supplemental Table 1. A summary of the differentially regulated pathways and genes identified by microarray cluster analyses from WT and MitoN-Tg sWAT. Gene abbreviations, definitions, in addition to fold-alterations and significant differences between WT and MitoN-Tg sWAT groups are indicated (n = 9 per group). *P < 0.05; **P < 0.01.

Pathway Gene	Gene definition	Fold-change	P-value
Adipogenic and lipogenic transcription factors:			
Pparγ	Peroxisome proliferator activated receptor γ	1.87	0.0067**
C/ebpα/β	CCAAT/enhancer-binding protein α/β	1.36/1.11	0.0458*/0.0382*
Srebp1c	Sterol regulatory element binding transcription factor 1	1.30	0.0500
Lxrα	Nuclear receptor subfamily 1, group H, member 3	1.30	0.0377*
Klf15	Kruppel-like factor 15	1.24	0.0429*
Adipo*q*	Adiponectin	1.50	0.0187*
TG synthesis, NEFA re-esterification and fatty acid biosynthesis:			
Lpin1	Lipin 1	1.31	0.0153*
Pepck-C	Phosphoenolpyruvate carboxykinase, soluble	1.52	0.0367*
Dgat1/2	Diacylglycerol O-acyltransferase 1	1.30/1.23	0.0580/0.0342*
Glut4	Solute carrier family 2 (facilitated glucose transporter) member 4	1.20	0.0138*
Gnpat	Glyceronephosphate O-acyltransferase	1.30	0.0343*
Fasn	Fatty acid synthase	1.20	0.0332*
Fads1/2	Fatty acid desaturase 1/2	1.57/1.20	0.0420*/0.0443*
Mcat	Malonyl CoA:ACP acyltransferase	1.26	0.0142*
Lipid-droplet associated proteins:			
Plin1	Perilipin 1	1.44	0.0374*
Fsp27	Cell death-inducing DFFA-like effector c	1.46	0.0291*
Fatty acid uptake, transport and oxidation:			
Fabp5	Fatty acid binding protein 5	1.50	0.0297*
Fatp4	Fatty acid transporter protein 4	1.20	0.0138*
Cd36	Cd36 antigen	1.15	0.0402*
Cpt1	Carnitine palmitoyl transferase I	-1.50	0.0057**
PPARα	Peroxisome proliferator activated receptor-α	-1.19	N.S
Beta-adrenergic signaling:			
Adrβ1/2/3	Adrenergic receptor β 1/2/3	1.18/1.09/1.36	N.S/N.S/0.0106*

Supplemental Table 2. A list of RT-PCR primer sequences of differentially expressed genes identified by the microarray cluster analysis from sWAT derived from WT mice versus MitoN-Tg mice.

Gene	Forward primer	Reverse primer
β-actin	5'-TACCACAGGCATTGTGATGG-3'	5'-TTTGATGTCACGCACGATTT-3'
Ppar-γ	5'-TCAGAGGGACAAGGATTCATGA-3'	5'-CACCAAAGGGCTTCCGCAGGCT-3'
C/ebp-α	5'-ACGCCGCCTTTGGCTTTC-3'	5'-TTGGCCTTCTCCTGCTGTCG-3'
C/ebp-β	5'-GCCAAGCCGAGCAAGAAGC-3'	5'-CAGGGCGAACGGGAAACC-3'
Adn	5'-GGAGATGCAGGTCTTCTTGG-3'	5'-CGAATGGGTACATTGGGAAC-3'
Pgc1-α	5'-TCCTCACACCAAACCCACAGAA-3'	5'-TTGGCTTGAGCATGTTGCGA-3'
Cd36	5'-TGAGACTGGGACCATTGGTGAT-3'	5'-CCCAAGTAAGGCCATCTCTACCAT-3'

Supplemental Table 3. *Ad libitum* chow-fed and fasted (24 h) body-weights and serum parameters in WT mice versus MitoN-Tg mice (n = 7 per group).

	Fed		Fasted (24 h)	
	WT	MitoN-Tg	WT	MitoN-Tg
Body-weight (g)	28.7 ± 0.9	28.2 ± 0.5	25.2 ± 1.1	24.9 ± 0.5
Glucose (mg/dl)	146.3 ± 5.2	138.7 ± 6.5	83.3 ± 5.0	100.1 ± 12.9
Insulin (ng/ml)	2.61 ± 0.40	1.85 ± 0.29	0.65 ± 0.05	0.78 ± 0.13
Triglyceride (mg/dl)	116.5 ± 17.3	36.9 ± 8.2**	63.1 ± 10.4	52.5 ± 6.6
FFA (mmol/l)	0.16 ± 0.02	0.12 ± 0.02	0.44 ± 0.03	0.58 ± 0.04*
Glycerol (mmol/l)	0.15 ± 0.02	0.16 ± 0.01	0.19 ± 0.01	0.26 ± 0.02**
Adiponectin (µg/ml)	6.8 ± 0.38	24.3 ± 1.18***	7.5 ± 0.29	21.7 ± 0.10***

Data obtained from 12-week old male FVB mice. ** P < 0.05; ** P < 0.01; *** P < 0.001.*

Supplemental Table 4. Chow-fed *ob/ob* mice versus MitoN-Tg *ob/ob* mice fasted (3 h) body-weights and serum parameters (n = 8 per group).

	ob/ob	MitoN-Tg *ob/ob*
Glucose (mg/dl)	427.4 ± 75.9	151.4 ± 17.2**
Insulin (ng/ml)	8.5 ± 2.9	5.4 ± 0.8
Triglyceride (mg/dl)	225.3 ± 58.0	94.1 ± 5.0*
Adiponectin (µg/ml)	6.7 ± 0.7	29.4 ± 2.4***

Data obtained from ~16-week old male FVB mice.
** P < 0.05; ** P < 0.01; *** P < 0.001.*

Supplementary Methods

Animals. Generation of an inducible shRNA-mitoN knockdown mouse model was developed as described by Seibler *et al.*[1] (Taconic Artemis). Briefly, the inducible shRNA transgene was constructed by introduction DNA encoding an shRNA of the sequence (5'-GGCCTTGCTACTGAAACATTTCAAGAGAATGTTTCAGTAGCAAGGCC-3') into a cassette consisting of a truncated Neomycin selectable marker, an H1-tetO promoter/operator for shRNA expression and a CAGGS-iTetR gene (for Dox-dependent repression of shRNA expression) all flanked by incompatible FRT sites for subsequent Flpe-mediated RMCE (Recombinase Mediated Cassette Exchange)[2] in ES cells. The 5' underlined 19 nucleotides are sense and the 3' underlined nucleotides are antisense to mitoNEET transcripts. The shRNA-mitoN transgene cassette was targeted to the RMCE compatible Rosa 26 locus in ES cells (strain 129S6). Six candidate shRNAs were tested in this transgenic format for optimal inducible knockdown of mitoNEET RNA in targeted ES cells. Targeted ES cells expressing the most potent shRNA molecule were utilized for generation of mice by blastocyst injection. Mice used in the present study have been backcrossed to C57/BL6 background. To generate a Dox-inducible mitoNEET overexpression mouse model, mitoNEET cDNA and a Kozak sequence of GCCGCCACC were engineered into the pTRE-tight vector (Clontech) with *Xba I* sites. The expression of mitoNEET is controlled by 7 tandem repeats of tetracycline responsive elements in front of a minimum CMV promoter in the pTRE-tight construct. A rabbit β-globin 3'UTR was included to stabilize the transcript and enhance the translation. After *Nae I*, and *ApaL I* digestion and purification, pTRE-mitoNEET DNA was injected to embryos into a pure C57/BL6 background by the transgenic core facility at UTSW. The liver specific albumin-Cre transgenic mice and the Rosa26-*loxP*-STOP-*loxP*-rtTA transgenic mice were purchased from the Jackson

Laboratories. Albumin-Cre mice were firstly bred with Rosa26-*loxP*-STOP-*loxP*-rtTA mice to obtain mice homozygous for both transgenes. To achieve inducible expression of mitoNEET, TRE-mitoNEET mice were then crossed with double homozygous albumin-Cre and Rosa26-*loxP*-STOP-*loxP*-rtTA mice. The resulting triple transgenic animals were used for experiments. Age-matched transgenic animals with albumin-Cre and Rosa26-*loxP*-STOP-*loxP*-rtTA genotype, but lacking the TRE-mitoNEET transgene were used as controls.

Transmission electron microscope (TEM). For TEM analysis, fresh tissues were fixed by perfusion with 4% paraformaldehyde and 1% glutaraldehyde in 0.1 M sodium cacodylate buffer. Fixed tissues were then transferred to 2.5% glutaraldehyde in 0.1 M sodium cacodylate buffer, post-fixed in buffered 1% osmium tetroxide, en bloc stained in 4% uranyl acetate in 50% ethanol, dehydrated with a graded series of ethanol, then embedded in EMbed-812 resin. Thin sections were cut on a Leica Ultracut UCT ultramicrotome and post-stained with 2% uranyl acetate and lead citrate. Images were acquired on a FEI Tecnai G^2 Spirit TEM equipped with a LaB_6 source and operating at 120 kV.

Primary hepatocyte isolation and treatment. Primary hepatocytes were isolated from 12-week old male C57/BL6 WT and shRNA-mitoN mice. Following overnight plating, hepatocytes were treated with either palmitate (400 μM) or MnTBAP (1 mg ml^{-1}) for 4 h, then acutely with insulin (16 mM) for 10 min. Protein was extracted for Western blot analysis.

Mitochondrial membrane potential (ΔΨm). For ΔΨm, WT MEFs and shRNA-mitoN MEFs ($1x10^5$) were incubated with or without Dox (1 μg ml^{-1}; 48 h). Cells were treated with 50 μM TMRM for 20 min at 37 °C, with an additional well containing control FCCP (20 μM for 30 min at 37 °C). All images were obtained using a confocal microscope (Leica TCS SP5) at 63×

magnification. In parallel, for stable transfection, the pCB7-mitoNEET construct was transfected into 3T3-L1 preadipocytes using Lipofectamine 2000 (Invitrogen). The transfected cells were selected by hygromycin B (125 μg ml^{-1}), then individual cell clones were isolated, expanded and analyzed for expression levels of recombinant mitoNEET protein by Western blot. Two clonal lines, with low- and high-mitoNEET expression levels respectively, were utilized for ΔΨm analysis, along with 3T3-L1 preadipocytes pre-treated for 12 h with 1.0 μM TZD (rosiglitazone) or control vehicle. ΔΨm was measured using 3,3′-dihexyloxacarbocyanine iodide ($DiOC_6$; Sigma) staining. Briefly, cultured cells were washed with PBS, then incubated for 15 min at 37 °C in 1 ml of serum-free culture medium containing 50 nM $DiOC_6$. Following centrifugation, cells were re-suspended in PBS, then immediately analyzed by flow cytometry on a FACscan (Becton Dickinson Immunocytometry Systems).

References

1. Seibler, J., *et al.* Reversible gene knockdown in mice using a tight, inducible shRNA expression system. *Nucleic Acids Res* **35**, e54 (2007).
2. Baer, A. & Bode, J. Coping with kinetic and thermodynamic barriers: RMCE, an efficient strategy for the targeted integration of transgenes. *Curr Opin Biotechnol* **12**, 473-480 (2001).